Global Biogeochemical Cycles

RESEARCH ARTICLE
10.1029/2024GB008163

Heat and Drought Events Alter Biogenic Capacity to Balance CO_2 Budget in South-Western Europe

R. Segura-Barrero[1], T. Lauvaux[2], J. Lian[3,4], P. Ciais[4], A. Badia[1], S. Ventura[1], H. Bazzi[5,6], E. Abbessi[4], Z. Fu[4], J. Xiao[7], X. Li[8], and G. Villalba[1,9]

[1]Sostenipra Research Group, Institute of Environmental Sciences and Technology, Universitat Autònoma de Barcelona (UAB), Barcelona, Spain, [2]Molecular and Atmospheric Spectrometry Group (GSMA)—UMR 7331, University of Reims Champagne Ardenne, Reims, France, [3]Origins Earth, Suez Group, Nanterre, France, [4]Laboratoire des Sciences du Climat et de l'Environnement (LSCE), IPSL, CEA-CNRS-UVSQ, Université Paris-Saclay, Gif-sur-Yvette, France, [5]AgroParisTech, INRAE, UMR 518 MIA Paris-Saclay, Université Paris-Saclay, Paris-Saclayf, France, [6]Atos France, Technical Services, Bezons, France, [7]Earth Systems Research Center, Institute for the Study of Earth, Oceans and Space, University of New Hampshire, Durham, NH, USA, [8]School of Geography and Planning, Sun Yat-sen University, Guangzhou, China, [9]Department of Chemical, Biological and Environmental Engineering, Universitat Autònoma de Barcelona (UAB), Barcelona, Spain

Abstract Heat and drought events are increasing in frequency and intensity, posing significant risks to natural and agricultural ecosystems with uncertain effects on the net ecosystem CO_2 exchange (NEE). The current Vegetation Photosynthesis and Respiration Model (VPRM) was adjusted to include soil moisture impacts on the gross ecosystem exchange (GEE) and respiration (R_{ECO}) fluxes to assess the temporal variability of NEE over south-western Europe for 2001–2022. Warming temperatures lengthen growing seasons, causing an increase in GEE, which is mostly compensated by a similar increment in R_{ECO}. As a result, there is a modest increase in the net carbon sink of 0.69 gC m^{-2} yr^{-1} but with high spatial and annual variability. The heatwave of 2022 reduced net carbon uptake by 91.7 TgC, a 26.4% decrease from the mean. The interannual variability of NEE is more influenced by drought in temperate humid regions than in Mediterranean semi-arid regions. These results emphasize the vulnerability of the net carbon sink as drying trends could revert the NEE trends, as it is happening for croplands in the French Central Massif.

Plain Language Summary Heat and drought events are increasing in frequency and intensity, posing significant risks to natural and agricultural areas, and altering their capacity for ecosystem CO_2 exchange. In view of recent heat and drought events, we study the changes in ecosystem carbon capture capacity and respiration over south-western Europe for 2001–2022. Warming temperatures lengthen growing seasons causing an increase in carbon capture which is mostly compensated by a similar increment in respiration, resulting in a modest annual increase of net carbon sink of 0.80 gC/m^2 yr^{-1} but with high spatial and annual variability such as the heatwave of 2022 which reduced the carbon sink by 27%. These results emphasize the vulnerability of the net carbon sink as drying trends could revert the carbon sink capacity, as it is happening for croplands in the French Central Massif.

Key Points:

- A modest annual increase of net carbon sink of 0.69 gC m^{-2} yr^{-1} is found in south-western Europe but with high spatial and annual variability
- The interannual variability in net ecosystem exchange is more influenced by drought in temperate humid regions than in Mediterranean semi-arid regions
- The heatwave and drought event of 2022 reduced net ecosystem exchange by 91.7 TgC, a 26.4% decrease from the mean

Supporting Information:

Supporting Information may be found in the online version of this article.

Correspondence to:

G. Villalba,
gara.villalba@uab.cat

Citation:

Segura-Barrero, R., Lauvaux, T., Lian, J., Ciais, P., Badia, A., Ventura, S., et al. (2025). Heat and drought events alter biogenic capacity to balance CO_2 budget in south-western Europe. *Global Biogeochemical Cycles*, *39*, e2024GB008163. https://doi.org/10.1029/2024GB008163

Received 13 MAR 2024
Accepted 20 DEC 2024

Author Contributions:

Conceptualization: R. Segura-Barrero, T. Lauvaux, J. Lian, P. Ciais, A. Badia, S. Ventura, H. Bazzi, E. Abbessi, Z. Fu, G. Villalba
Formal analysis: R. Segura-Barrero, T. Lauvaux, J. Lian, P. Ciais, A. Badia, S. Ventura, H. Bazzi, E. Abbessi, Z. Fu, G. Villalba
Funding acquisition: R. Segura-Barrero, T. Lauvaux, S. Ventura, H. Bazzi, E. Abbessi, Z. Fu, G. Villalba

1. Introduction

Global climate change, particularly increasing extreme climate events, is profoundly impacting the terrestrial carbon balance and altering vegetation dynamics (Ciais et al., 2005; Keenan et al., 2016; Reichstein et al., 2013). Climate warming has extended the growing season in Northern ecosystems by producing more favorable conditions for photosynthesis, thereby increasing their terrestrial ecosystem productivity or gross ecosystem exchange (GEE) (Ciais et al., 2019; Zhu et al., 2016). The increased atmospheric carbon dioxide (CO_2) concentrations also have positive fertilization effects on the vegetation productivity (Los, 2013; Schimel et al., 2015; Thornton et al., 2007). However, warming has also stimulated the release of terrestrial carbon to the atmosphere or ecosystem respiration (R_{ECO}) by enhancing soil organic matter decomposition and vegetation respiration (Keenan et al., 2016). Interannual variations of these biogenic carbon fluxes are expected to increase with increasing frequency and intensity of extreme climate events (Zscheischler, Mahecha, et al., 2014; Zscheischler, Reichstein, et al., 2014), potentially destabilizing the long-term carbon cycle (Fernández-Martínez et al., 2023).

Investigation: R. Segura-Barrero, T. Lauvaux, J. Lian, P. Ciais, H. Bazzi, E. Abbessi, Z. Fu, G. Villalba
Methodology: R. Segura-Barrero, T. Lauvaux, J. Lian, P. Ciais, A. Badia, S. Ventura, H. Bazzi, E. Abbessi, Z. Fu, G. Villalba
Resources: R. Segura-Barrero, T. Lauvaux, S. Ventura, H. Bazzi, E. Abbessi, Z. Fu, G. Villalba
Software: R. Segura-Barrero, H. Bazzi, E. Abbessi, Z. Fu, G. Villalba
Supervision: R. Segura-Barrero, T. Lauvaux, J. Lian, P. Ciais, A. Badia, S. Ventura, H. Bazzi, E. Abbessi, Z. Fu, G. Villalba
Validation: R. Segura-Barrero, H. Bazzi, E. Abbessi, Z. Fu, J. Xiao, X. Li, G. Villalba
Visualization: A. Badia, S. Ventura, H. Bazzi, E. Abbessi, Z. Fu, G. Villalba
Writing – original draft: R. Segura-Barrero, H. Bazzi, E. Abbessi, Z. Fu, G. Villalba
Writing – review & editing: R. Segura-Barrero, T. Lauvaux, J. Lian, P. Ciais, A. Badia, S. Ventura, H. Bazzi, E. Abbessi, Z. Fu, J. Xiao, X. Li, G. Villalba

Regions like south-western Europe, which experience transitional climate conditions, are especially sensitive to warming and drying trends (Giorgi & Lionello, 2008). These conditions exacerbate the impacts of extreme climate events such as heat and drought events (Fischer & Schär, 2010; Molina et al., 2020), which pose significant risks to crops, forests, and overall ecosystem carbon balance. Although the Mediterranean climate is typically characterized by long dry summers (Gilabert et al., 2015), the resilience of its forests (Bento et al., 2023; Gazol et al., 2018) and crops (Alonso et al., 2019; Ribeiro et al., 2019) reaches its limits when long drought episodes combined with heat waves start to affect the plants (Ermitão et al., 2021; Rita et al., 2020). The occurrence of heatwaves and droughts, and the associated disturbances can partially reduce the net atmospheric carbon uptake or net ecosystem exchange (NEE) or even cause net losses in carbon stocks, releasing CO_2 to the atmosphere (Qu et al., 2024; Reichstein et al., 2013). For instance, the exceptional drought of the summer 2022, affecting central and south-eastern Europe, caused a reduction of the net biosphere uptake over the drought area in summer between 56 and 62 TgC (van der Woude et al., 2023). It is crucial to comprehend the impact of heat and drought events on the south-western European carbon balance, given its vulnerability to climate change (Fischer & Schär, 2010; Giorgi & Lionello, 2008; Molina et al., 2020).

A multi-year analysis of the impact of drought and heat events on biogenic carbon fluxes is essential for south-western Europe, where long-term observational records of CO_2 concentrations and fluxes are sparse. This gap limits our understanding of regional carbon dynamics, particularly the intricate dependencies of GEE and R_{ECO} on heat and drought episodes (Reichstein et al., 2013; von Buttlar et al., 2018). Although numerous studies have investigated the role of water and heat stress on vegetation productivity and GEE in southern Europe (Ermitão et al., 2021; Gilabert et al., 2015; Gouveia et al., 2017; Rita et al., 2020), changes in the NEE remains highly uncertain due to overlooked complex dependencies from heat and drought episodes on R_{ECO}. Additionally, soil water availability and vapor pressure deficit (VPD; atmospheric dryness) are the main factors driving interannual variability of photosynthesis (Gilabert et al., 2015), yet the timing of drought and heat events is also an important factor regulating the vegetation response (Jin et al., 2023). Moreover, process-based biogeochemical models usually fail to capture the vegetation carbon response to extreme variations in soil moisture (Stocker et al., 2018, 2019).

Remote sensing data-driven biosphere models, which estimate ecosystem fluxes based on satellite-derived vegetation indices and meteorological drivers, usually estimate the water stress effect on GEE using satellite sensed water indices or VPD without considering soil moisture as a model input (Fu et al., 2022; Running et al., 2004; Stocker et al., 2018, 2019). Although satellite-derived vegetation indices based on vegetation structure (i.e., the Normalized Difference Vegetation Index, NDVI, or the Enhanced Vegetation Index, EVI) can to some extent capture the effect of droughts on GEE (Maselli et al., 2009), they tend to underestimate the magnitude of GEE reductions under dry conditions (Stocker et al., 2019). For instance, the Vegetation Photosynthesis and Respiration Model (VPRM) (Mahadevan et al., 2008) does not consider soil moisture as a constraint (Mahadevan et al., 2008). Different studies have shown the potential of enhancing the VPRM model capabilities by model parameter optimization (Dayalu et al., 2018) or by modifying the respiration equation (Gourdji et al., 2022), resulting in similar or even better model performances compared to more complex process-based models.

The main objective of this study is to determine the effect of heat and drought events on the temporal variability of the net biogenic carbon fluxes over south-western Europe, including Portugal, Spain, southern France, and Italy, for the period 2001–2022. To do so, we modify the VPRM model to incorporate the impact of soil moisture on the GEE and R_{ECO}. In addition to the analysis of long-term carbon flux variability over this whole period, we also examine the control of climate driver anomalies (temperature, soil moisture and solar radiation) and a drought index, the Standardized Precipitation Evaporation Index (SPEI) (Vicente-Serrano et al., 2010, 2013), on the interannual anomalies of carbon fluxes over 10 biogeographical regions (Figure 1). To complement the analysis of VPRM simulations, we also use GEE based on the sun-induced chlorophyll fluorescence (SIF), a Global Orbiting Carbon Observatory-2 (OCO-2) SIF product (GOSIF) (Li & Xiao, 2019) between 2001 and 2022, and carbon flux estimates from the process-based biogeochemical model ORCHIDEEv3 (McGrath et al., 2023). Finally, we study the intra-annual variations in carbon fluxes in the following regions during two exceptional heat and drought events: the Iberian sclerophyllous region in the year 2005, and the Atlantic region in the year 2022.

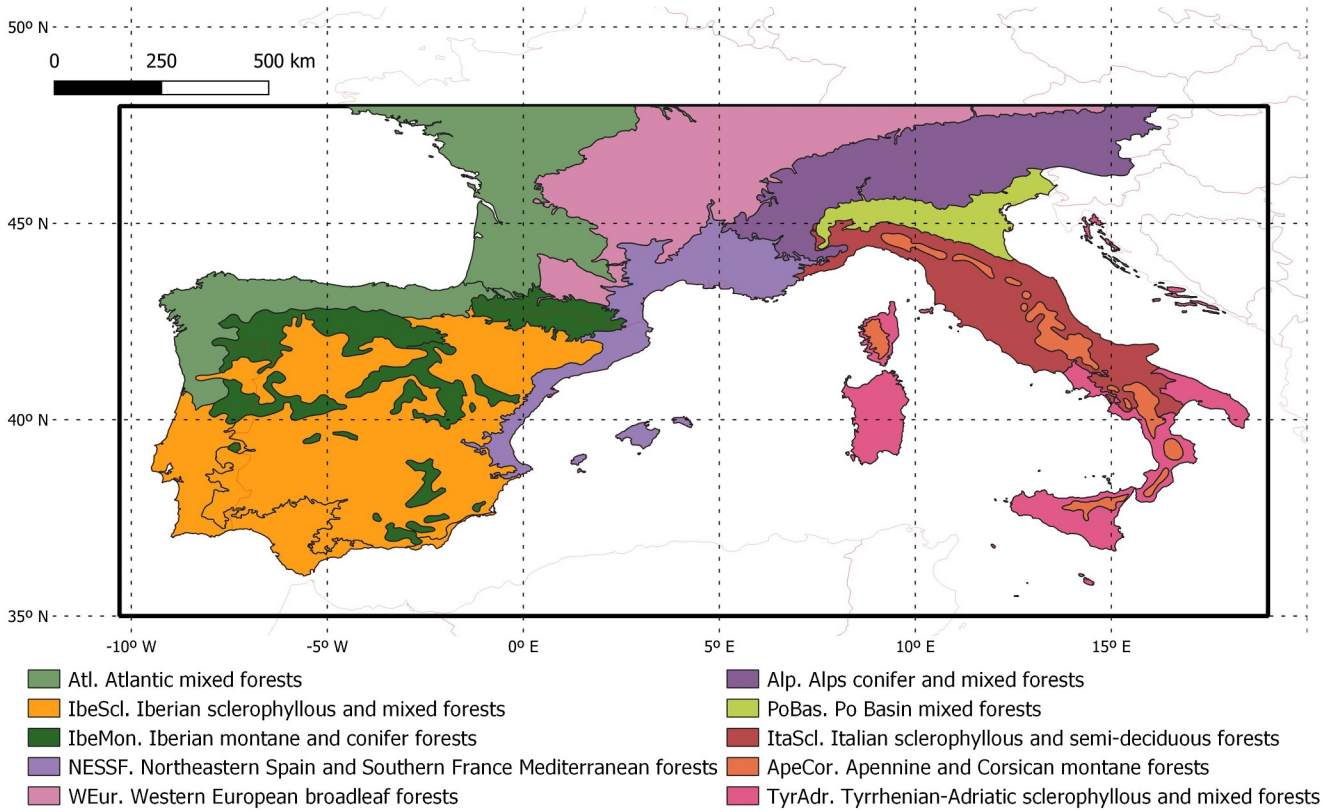

Figure 1. Biogeographical regions. Area of study and biogeographical regions of this study.

2. Materials and Methods

2.1. Study Area

The study region encompasses south-western Europe from Portugal to Italy (Figure 1). This large area encompasses a great diversity of ecosystems, topographical features, climates, land-use, and soil typologies (Gouveia et al., 2017), which we classify into 10 biogeographical regions based on the map of Terrestrial Ecoregions of the World from the World Wildlife Fund (Olson et al., 2001). The classification of the biogeographical regions is detailed in Supporting Information S1. The prevailing climate is the subtropical Mediterranean climate with hot and dry summers, although other climates such as temperate oceanic, mountainous and humid continental climates are present.

2.2. VPRM Modifications

VPRM simulates surface CO_2 exchanges between the atmosphere and the biosphere using meteorological data and remote-sensing vegetation indices (cf. Supporting Information S1). NEE is estimated as the difference between R_{ECO} and GEE, following a negative sign convention where negative fluxes represent CO_2 uptake by ecosystems. VPRM parameters are optimized for 8 plant functional types (PFT) representing various land cover types (i.e., evergreen forest, deciduous forest, mixed forest, shrubland, Mediterranean savanna, cropland, grassland, and sparsely or non-vegetated), weighted by fractional coverage to calculate the regional ecosystem fluxes.

To account for the impact of soil moisture on GEE and R_{ECO}, modifications were made in the VPRM equations, with an R_{ECO} parameterization based on a previous study (Migliavacca et al., 2011). The methodology for optimizing the modified and default VPRM parameters using data from southern Europe flux tower observations is presented in Supporting Information S1. The flux tower data is obtained from the data sets FLUXNET 2015 (Pastorello et al., 2020) and the Warm Winter 2020 product from ICOS (Warm Winter 2020 and ICOS Ecosystem Thematic Centre, 2022) (see Figure S1 and Tables S1 and S2 in Supporting Information S1).

The GEE parameterization consists of a light-use-efficiency approach that relates the GEE to the fraction of photosynthetically active radiation that is absorbed by vegetation canopies, combined with a set of optimized scaling factors (λ_{SW}, T_{scale}, W_{scale}, and P_{scale}). We introduce a new scaling factor, SM_{scale}, to better represent soil moisture stress on GEE, distinguishing between adequate soil water and insufficient soil water regimes, according to a previous study (Stocker et al., 2019). The GEE parameterization is defined as

$$GEE = \lambda_{SW} \cdot T_{scale} \cdot W_{scale} \cdot P_{scale} \cdot SM_{scale} \cdot \frac{SW}{(1 + SW/SW_0)} \cdot EVI \quad (1)$$

where SW is shortwave radiation, and SW_0 is the half-saturation shortwave radiation. The function SM_{scale} is defined to be 1 when the soil moisture (θ) is above a critical soil moisture threshold (θ^*) and decreases linearly below this threshold (Fu et al., 2022). Soil moisture in the uppermost soil level (0–15 cm depth) is normalized between the permanent wilting point and the field capacity of the soil. The form of the SM_{scale} function is:

$$SM_{scale} = \begin{cases} q \cdot (\theta - \theta^*) + 1, \theta < \theta^* \\ 1, \theta \geq \theta^* \end{cases} \quad (2)$$

where q and θ^* are optimized parameters, being q the sensitivity of GEE to low soil moisture. With this modification, we increase the number of parameters in the GEE parameterization from two (λ_{SW}, SW_0) to four (adding q and θ^*).

The default VPRM employs a linear function of air temperature to determine R_{ECO}. In this study, we use an equation proposed in two previous studies (Migliavacca et al., 2011; Reichstein et al., 2003). In our approach, we employ soil moisture rather than precipitation to depict water stress on R_{ECO} using a hyperbolic tangent function. This choice is due to soil moisture's superior role in influencing soil microbial processes and plant stress (W. Liu et al., 2009). The R_{ECO} equation in the modified VPRM relies on air temperature, soil moisture and short-term vegetation productivity (daily GEE) as follows:

$$R_{ECO} = (R_0 + k_1 \cdot GEE) \cdot \tan h(k_2 \cdot \theta + \gamma) \cdot e^{E_0 \cdot \left(\frac{1}{T_{ref} - T_0} - \frac{1}{T - T_0}\right)} \quad (3)$$

GEE represents the average GEE over the previous 24 hr, and T is the air temperature. T_{ref} and T_0 are fixed temperatures at 288.15 K (15°C) and 227.13 K (−46.02°C), respectively. Model-specific constants, R_0, k_1, k_2, γ, and E_0 vary for each PFT and refer to reference abiotic ecosystem respiration, sensitivity of R_{ECO} to GEE, sensitivity of R_{ECO} to soil moisture, a constant indicating how R_{ECO} responds to null θ, and the activation energy parameter for the sensitivity of R_{ECO} to air temperature, respectively. Including vegetation productivity in the respiration parameterization enhances the spatial and temporal dynamics of R_{ECO}, preventing a bias in seasonal amplitude (Migliavacca et al., 2011). GEE has also been included in previous studies to improve the estimation of R_{ECO} (Xiao et al., 2011, 2014).

The VPRM model is used to estimate biogenic carbon fluxes (NEE, GEE, and R_{ECO}) at an hourly resolution spanning from 2001 to 2022 and at a spatial resolution of 9 km. The model uses meteorological drivers from the ERA5-Land data set (Muñoz-Sabater, 2019) and satellite-derived vegetation indices processed from MODIS surface reflectances (Vermote, 2015). The model computes fluxes individually for each PFT and results were subsequently aggregated based on the VPRM PFT map. Another modification to VPRM includes differentiating between summer and winter crops within the cropland PFT, as is explained in Supporting Information S1.

2.3. Climate and Remotely Sensed Data

Climatic driver data are from the European Centre for Medium-Range Weather Forecasts (ECMWF) ERA5-Land reanalysis product. These data cover the years from 1950 to present, with hourly frequency and 0.1° resolution (Muñoz-Sabater, 2019). For this study, only the data from 2001 to 2022 is used. The key variables used include 2 m temperature (T2M) for air temperature, surface solar radiation downwards (SSRD) for shortwave radiation, and volumetric soil water of the second layer (7–28 cm depth; SM2) for soil moisture. This specific soil layer is

chosen because of its higher correlation with observed soil water content from flux tower stations compared to other layers.

To assess drought episodes across south-western Europe, monthly averaged ERA5-Land variables, including T2M, SSRD, and SM2, are employed. Additionally, the multi-scalar drought index SPEI is computed at various month aggregations (1-, 3-, 6-, 9- and 12-month, for SPEI01, SPEI03, SPEI06, SPEI09, and SPEI12, respectively) to assess drought intensity and variability using monthly averaged ERA5-Land data between 1951 and 2022. SPEI considers not only precipitation but also the atmospheric evaporative demand crucial for studying vegetation impacts on warm regions (Vicente-Serrano et al., 2010, 2013). The SPEI is determined based on a log-logistic probability distribution of the series of differences between precipitation and potential evapotranspiration (PET), with PET calculated using the Food and Agriculture Organization (FAO-56) Penman-Monteith equation. The Python module SPEI (Vonk, 2024) is used for the derivation of the drought index.

The EVI and the land surface water index (LSWI) are processed from the MODIS Terra satellite MOD09A1 v6.1 product (Vermote, 2015) using the VPRM preprocessor from the Department of Biogeochemical Systems in the Max Planck Institute for Biogeochemistry (https://www.bgc-jena.mpg.de/4758306/bsi_vprmpreproc; last access 22/11/2024).

The VPRM model uses the Synergetic Land Cover Product (SYNMAP) (Jung et al., 2006) for the vegetation classification map reclassified to the 8 VPRM PFTs. SYNMAP is a 1-km global land cover product built from remote sensing observations and its classes are defined based on PFT mixtures with explicit leaf type and longevity definitions, and thereby is ideal for carbon cycle modeling applications.

To complement the analysis of VPRM simulations, we also use GEE based on the SIF product GOSIF (0.05°) between 2001 and 2022 (Li & Xiao, 2019). GOSIF GEE exhibits strong correlations with flux tower GEE at 8-day, monthly, and annual scales, maintaining a high correlation with GEE even during drought episodes (Lv et al., 2023; Qiu et al., 2022), and offers the advantage of relying solely on satellite SIF observations, eliminating the need for climate data.

GEE, R_{ECO}, and NEE are also estimated using the process-based ORCHIDEEv3 model at high-resolution (0.125°) over Europe simulating between 1901 and 2022 (McGrath et al., 2023). ORCHIDEE estimates carbon, water and energy fluxes from environmental drivers (meteorology and CO_2 mole fractions) including a dynamic nitrogen cycle coupled to the vegetation carbon cycle. ORCHIDEE is driven with meteorological data from ERA5-Land realigned with the Climatic Research unit (CRU) observation data set at 0.5° between 1981 and 2022, and is driven with the UERRA HARMONIE-V1 data set realigned with the CRU between 1901 and 1981 as described in McGrath et al. (2023).

2.4. Statistical Analysis

Monthly anomalies of GEE, R_{ECO}, NEE and the climate drivers (T2M, SM2, and SSRD) are calculated, as the difference between monthly values and monthly means for the entire period 2001–2022. The methodology used to determine the long-term trend of consists of a linear regression of the carbon flux annual anomaly time series and the significance of these trends is assessed using a Pearson correlation test.

To investigate the influence of SPEI at various timescales on the interannual variability of fluxes, a Pearson correlation analysis is conducted using the time series of detrended flux anomalies. In the case of the climate drivers, the partial correlation coefficient is calculated for each variable controlling the interannual variations in the other two driver variables. For this analysis, detrended anomalies are aggregated for growing season months, identified for each biogeographical region and based on average seasonal cycles. Growing season months are determined based on when the monthly mean GOSIF GEE exceeds 30% of the intra-annual GEE range (Figure S1 in Supporting Information S1). Although GOSIF GEE and VPRM GEE generally exhibit similar seasonal cycles across all biogeographical regions, discrepancies are observed for the Iberian and Tyrrhenian-Adriatic sclerophyllous regions. Higher discrepancies are observed with ORCHIDEE GEE, which presents earlier growing seasons (Figure S1 in Supporting Information S1).

Finally, we select two study cases consisting of years with severe heat and drought events largely affecting the NEE of the south-western European ecosystems to study intra-annual variations in biogenic carbon fluxes in response to these major events. The study cases are the Iberian sclerophyllous region in the year 2005, and the

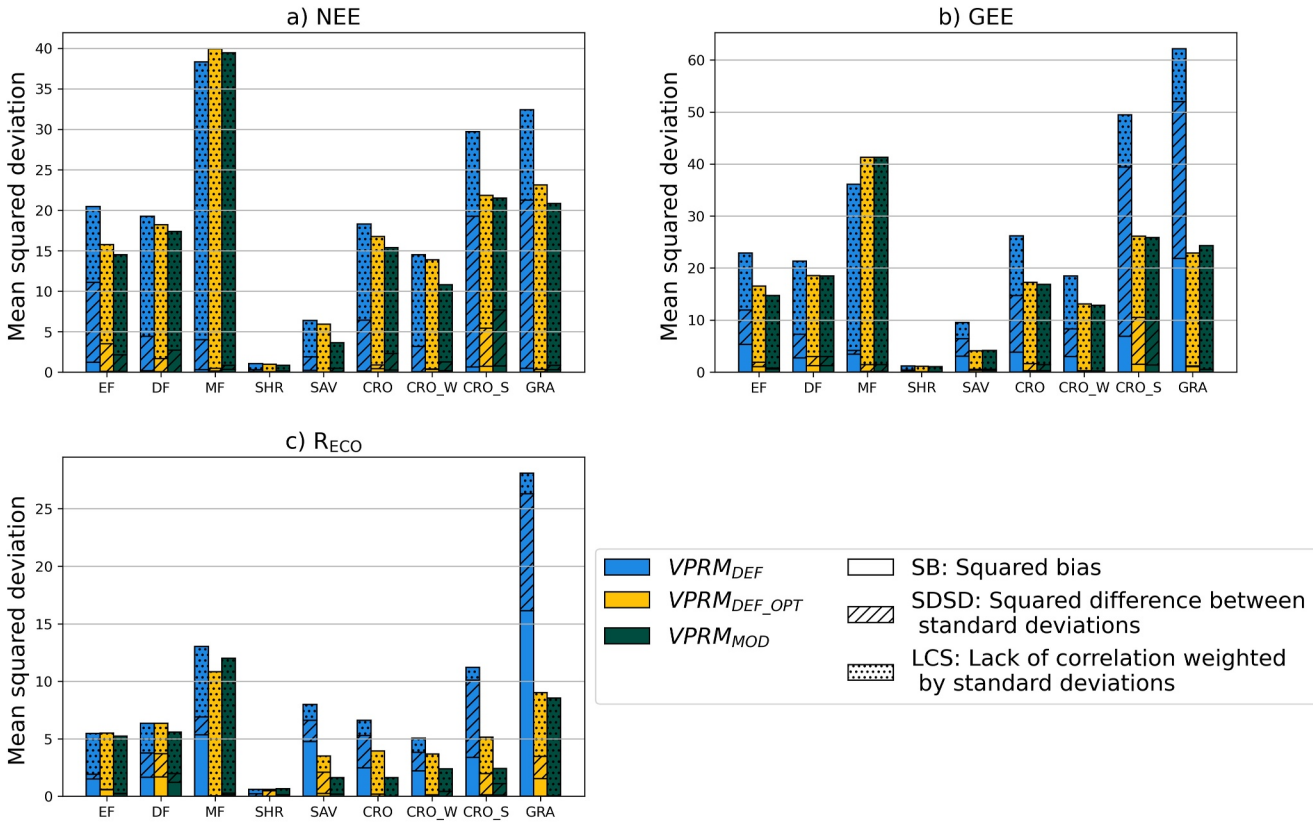

Figure 2. Decomposed mean squared deviation comparison. Mean squared deviation (MSD) and its components SB, SDSD, and LCS for the three VPRM versions calculated using half hourly data and the different PFTs. (a) NEE, (b) GEE, and (c) R_{ECO}. EF: evergreen forest, DF: deciduous forest, MF: mixed forest, SHR: shrubland, SAV: savanna, CRO: cropland, CRO_W: winter crops; CRO_S: summer crops; GRA: grassland.

Atlantic region in the year 2022. For these study cases, VPRM-simulated carbon fluxes, along with T2M and SM2, are aggregated on an 8-day basis. Anomalies relative to the means over the 2001–2022 period are computed for each grid cell and 8-daily period within the year.

3. Results

3.1. Performance Evaluation of the Different Versions of VPRM With Flux Tower Data

In this section, we compare the performances of the default VPRM ($VPRM_{DEF}$, see Supporting Information S1), the default VPRM with optimized parameters ($VPRM_{DEF\_OPT}$) and the modified VPRM ($VPRM_{MOD}$) for simulating the CO_2 fluxes over eddy-covariance flux towers in south-western Europe, using half-hourly observed fluxes (NEE), and GEE and R_{ECO} estimates from observations using the nigh-time partitioning method (Pastorello et al., 2020). An evaluation data set subset of flux tower observations is employed (Table S2 in Supporting Information S1). The statistical metrics used for the evaluation of the model-data fitting are the Pearson correlation coefficient (r), the Root Mean Squared Error (RMSE) and the Mean Squared Deviation ($MSD = RMSE^2$) decomposed as the sum of three components: the squared bias (SB), the squared difference between measured and simulated standard deviation (SDSD) and the lack of correlation weighted by the standard deviation (LCS). Further details of the MSD decomposition are explained in Kobayashi and Salam (2000).

Regarding the NEE, $VPRM_{MOD}$ exhibits lower RMSE (Figure S3a in Supporting Information S1) and stronger correlations with observations (Figure S4a in Supporting Information S1) across most PFTs except for mixed forest. Optimizing VPRM parameters achieves significant RMSE reductions (exceeding 0.55 μmol CO_2 m^{-2} s^{-1}) for evergreen forest, summer crops, and grasslands (Figure S3a in Supporting Information S1). The improved performance of $VPRM_{DEF\_OPT}$ and $VPRM_{MOD}$ results from a close match in the standard deviation of the modeled NEE to the observed values compared to $VPRM_{DEF}$ (Figure 2a). An evaluation of the seasonal cycles

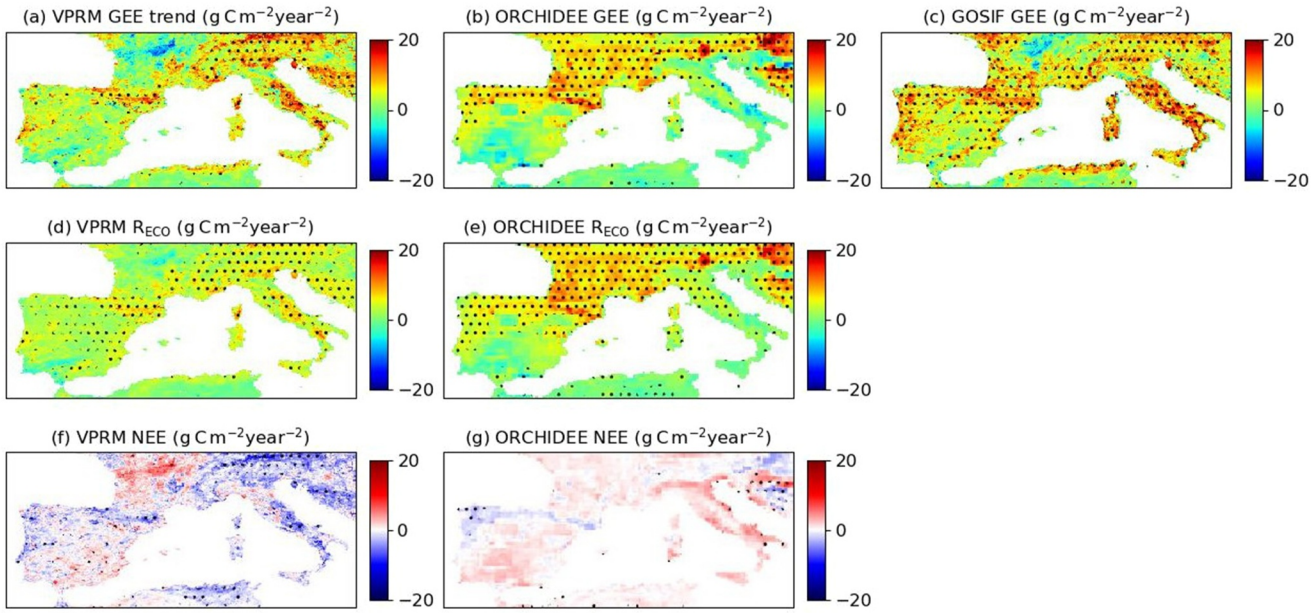

Figure 3. Long-term carbon flux trends. Spatial pattern of the long-term trends of annual fluxes for (a) VPRM GEE; (b) ORCHIDEE GEE; (c) GOSIF GEE; (d) VPRM R_{ECO}; (e) ORCHIDEE R_{ECO}; (f) VPRM NEE; (g) ORCHIDEE NEE between 2001 and 2022. The black dots correspond to areas where the linear regression is significant ($p < 0.05$).

with monthly mean fluxes (Figure S5 in Supporting Information S1), reveals that all versions closely match the observed negative peak during the growing season for all PFTs except Mediterranean savannas, where $VPRM_{MOD}$ aligns more closely with the observations than $VPRM_{DEF}$ and $VPRM_{DEF\_OPT}$.

Regarding the GEE, $VPRM_{MOD}$ presents the lowest RMSE for evergreen forest, with notable reductions achieved through parameter optimization (Figure S3b in Supporting Information S1). $VPRM_{MOD}$ exhibits the strongest correlations with the observations for evergreen forest, shrubland and winter crops (Figure S4b in Supporting Information S1), although similar correlations are found for the other PFTs. The optimization of the VPRM parameters decreases SB and SDSD across all PFTs except mixed forests (Figure 2b), while increasing LCS implies a better estimation of the magnitudes of the fluctuations of GEE. The VPRM parameter optimization improves the representation of the growing season GEE peaks in all PFTs except mixed forests (Figure S5 in Supporting Information S1). The differences in GEE seasonal cycles between $VPRM_{DEF\_OPT}$ and $VPRM_{MOD}$ are not significant, indicating minor impact from GEE parameterization modifications at the monthly scale (Figure S5 in Supporting Information S1).

Regarding the R_{ECO}, $VPRM_{MOD}$ generally has lower RMSE (Figure S3c in Supporting Information S1) and stronger correlation with observations (Figure S4c in Supporting Information S1), except for mixed forest and shrubland where $VPRM_{DEF\_OPT}$ outperforms. $VPRM_{MOD}$ significantly improves model data-fitting for savannas, croplands (in all aggregations) and grasslands, with RMSE reductions exceeding 0.71 μmol CO_2 m^{-2} s^{-1}. The improvements shown for $VPRM_{MOD}$ stem from the reduction of the SB and SDSD for all the PFTs as well as the reduction of the LCS for savannas and croplands. $VPRM_{MOD}$ better captures peak seasonal cycles for deciduous forest, savanna, croplands, and grasslands compared to $VPRM_{DEF\_OPT}$ and $VPRM_{DEF}$ (Figure S5 in Supporting Information S1). Introducing GEE in the R_{ECO} parameterization corrects the timing of the seasonal peak for savannas and croplands.

Based on the better performance of the modified VPRM for most of the PFTs, we will focus solely on this version of VPRM and refer to it from now on as VPRM.

3.2. Trends of South-Western Europe Carbon Fluxes

The long-term trend analysis of carbon fluxes from VPRM, ORCHIDEE, and GOSIF shows an overall increase of both GEE and R_{ECO}, with certain regions showing flux stability (Figure 3). GOSIF presents a positive trend in

GEE (spatial median of 5.50 g C m^{-2} $year^{-2}$ and 52.5% of the vegetated areas showing significant increases), while positive VPRM GEE trends are more localized to the mountainous regions (3.58 g C m^{-2} $year^{-2}$ and 25.3%). Both models are consistent in estimating a non-significant negative trend in the GEE in the Massif Central mountains (south-central France). ORHCIDE GEE spatial median trends (3.58 g C m^{-2} $year^{-2}$ and 43.2% of the domain) align with the VPRM spatial median trend, but spatial distributions differ. ORCHIDEE estimates positive trends in the French Massif Central, and negative or near-zero trends across the Italian peninsula.

The long-term trends of the VPRM R_{ECO} present a similar spatial distribution to those of GEE, although the magnitude (spatial median of 3.01 g C m^{-2} $year^{-2}$) is smaller than that for the GEE (3.58 g C m^{-2} $year^{-2}$). The spatial extent of the areas with significant VPRM R_{ECO} trends (36.0%) extends further than the areas with significant GEE trends (25.3%). ORCHIDEE R_{ECO} trends are spatially distributed similar to ORCHIDEE GEE trends but with higher spatial magnitude and extent (spatial median of 4.02 g C m^{-2} $year^{-2}$, and 61.4%).

The comparable spatial trends of VPRM GEE and R_{ECO} reflect that long-term variations in released and captured carbon by the ecosystems compensate each other, implying a trend approaching zero in the NEE (-0.69 g C m^{-2} $year^{-2}$ and 14.6%) (Figure 2d). VPRM estimates a significant increase of net carbon sink over specific regions located in the Alps (-2.39 g C m^{-2} $year^{-2}$), and the Apennines, and Corsican (-3.43 g C m^{-2} $year^{-2}$) mountainous regions (Figure S6 in Supporting Information S1). Only one region, located in the northern part of the Massif Central, shows a non-significant decrease in net carbon sink (maximum trends of 11.33 g C m^{-2} $year^{-2}$). On the contrary, ORCHIDEE estimates a positive and non-significant trend in the NEE (0.51 g C m^{-2} $year^{-2}$ and 5.2%). High disagreement between ORCHIDEE and VPRM is found in the Italian peninsula and the Alps (Figures 3f and 3g).

The disaggregation of the fluxes by PFT reveals that the increase in the long-term trends of the GEE and R_{ECO} in the Po Basin, the Italian sclerophyllous, the Apennine and Corsican montane and the Tyrrhenian-Adriatic sclerophyllous regions is dominated by croplands (Figure 4). In other regions such as the Atlantic, the Iberian sclerophyllous and the Western European broadleaf regions, the long-term trends of R_{ECO} are higher than those for the GEE in croplands, counteracting the contributions of the natural PFTs with stronger sink increases.

Over the entire study area (Figure 5), VPRM, ORCHIDEE, and GOSIF GEE shows a significant increase of 6.5, 6.6, and 9.4 Tg C $year^{-2}$, respectively. GOSIF and VPRM GEE show strong agreement on the interannual variability. VPRM and ORCHIDEE R_{ECO} also exhibit a significant increase of 5.0 and 7.7 Tg C $year^{-2}$, respectively, with high agreement on the interannual variability. This occurs in conjunction with a significant warming trend of 0.057°C $year^{-1}$ and a non-significant soil drying trend over the region. Due to the compensation between GEE and R_{ECO}, the VPRM NEE shows a non-significant decrease of -1.5 Tg C $year^{-2}$, while ORCHIDEE presents a non-significant increase of 1.1 Tg C $year^{-2}$. This discrepancy between models is caused by the different R_{ECO} trends. Moreover, the occurrence of summer heat and drought events increases the intra-annual variability of NEE, producing the largest positive NEE anomalies.

3.3. Interannual Variability of Carbon Fluxes

Figure 6 shows the correlation between VPRM GEE and R_{ECO} interannual anomalies and the SPEI01, SPEI03, and SPEI06, and the partial correlation of the flux anomalies with the climate drivers (T2M, SM2, and SSRD) during the growing season months. Water availability prevails as the dominant driver of GEE interannual variability. Except for the Alps, the strongest correlations with GEE anomalies are found for SPEI (spatial median ranges between 0.37 and 0.76) and soil moisture (between 0.35 and 0.64). These results suggest that seasonal and extended droughts significantly influence GEE fluctuations. The correlations of GEE with SPEI at higher timescale aggregations (9 and 12 months) (between 0.29 and 0.73) are slightly lower than those for lower timescale (Figure S7 in Supporting Information S1). GEE in Mediterranean climate biogeographical regions (IbeScl., IbeMon., NESSF., TyrAdr.) shows a higher correlation with SPEI06, while in temperate humid regions, GEE presents higher correlations with SPEI03 (Atl., WEur., ItaScl., ApeCor.) or SPEI01 (PoBas.). The strongest correlations between SPEI and GEE anomalies are found in the Iberian sclerophyllous and Tyrrhenian-Adriatic regions (Figure 6), specifically for SPEI06 ($r = 0.76$ for IbeScl., and $r = 0.72$ for TyrAdr.).

In low-altitude regions (excluding Alps, Apennine, and Corsican montane forests), air temperature shows primarily non-significant negative partial correlations with GEE anomalies (between -0.28 and 0.02), while R_{ECO}

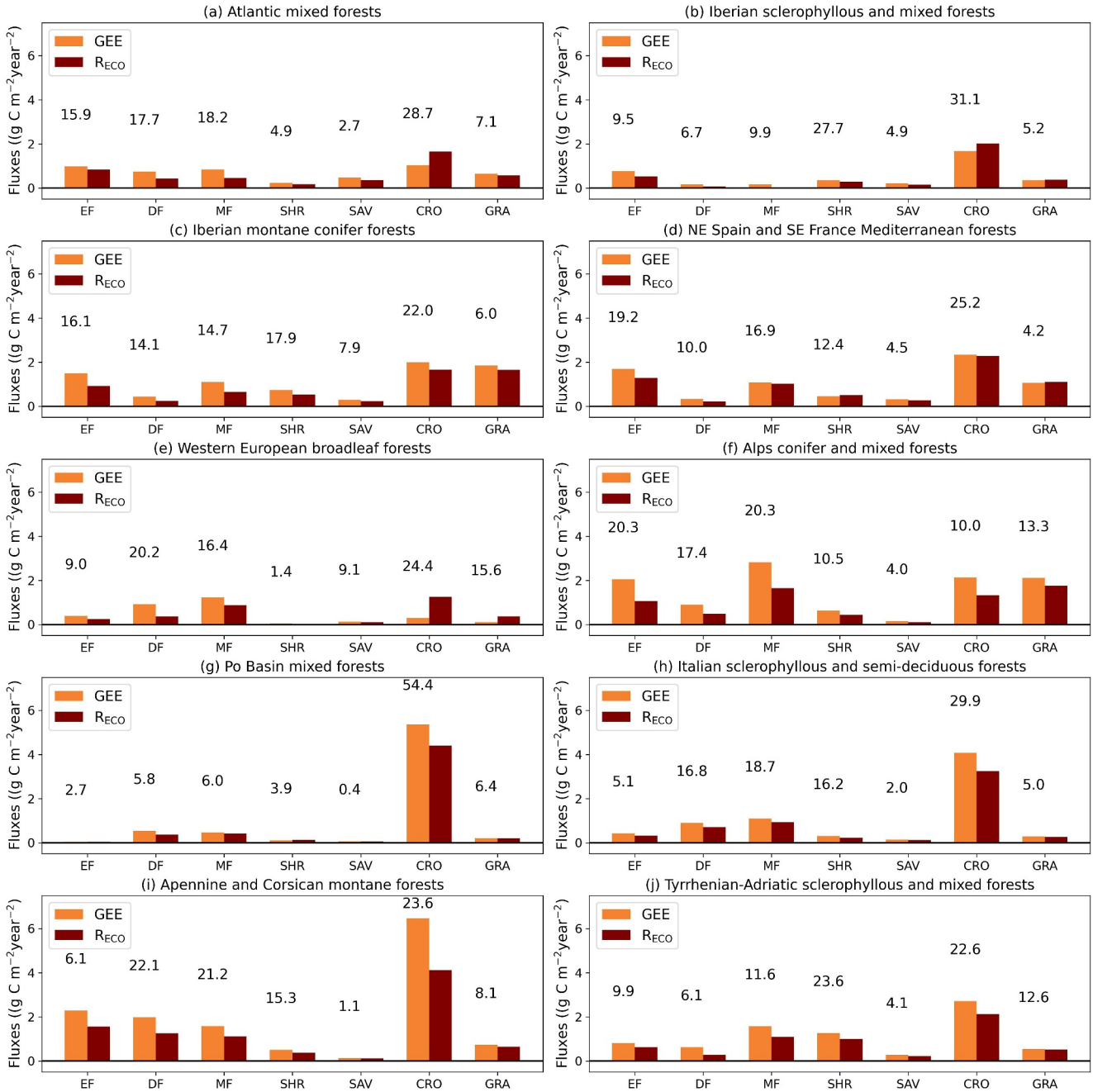

Figure 4. Long-term carbon flux trends by PFT. Average trends of the VPRM GEE and R_{ECO} aggregated annually for the different biogeographical regions and integrated for the different plant functional types. The PFT percent coverage is marked over each bar.

shows positive partial correlations with air temperature (between 0.04 and 0.42). Higher temperatures during the growing season lead to reduced gross CO_2 uptake and increased CO_2 release, while increased precipitation and soil moisture promote the photosynthetic activity. Although radiation presents a positive correlation with GEE, it is generally non-significant (between 0.03 and 0.27). In temperate humid regions such as the Atlantic, Western Europe and Po Basin, R_{ECO} displays weaker correlations with SPEI01 (r = 0.15–0.42) compared with GEE (SPEI: r = 0.43–0.62), indicating that R_{ECO} is less sensitive to droughts in such regions. Conversely, in south-eastern regions like Tyrrhenian-Adriatic, Apennine and Corsican montane, R_{ECO} exhibits stronger correlations with SPEI and partial correlations with soil moisture (SPEI: r = 0.53–0.81; SM2: r = 0.62–0.79).

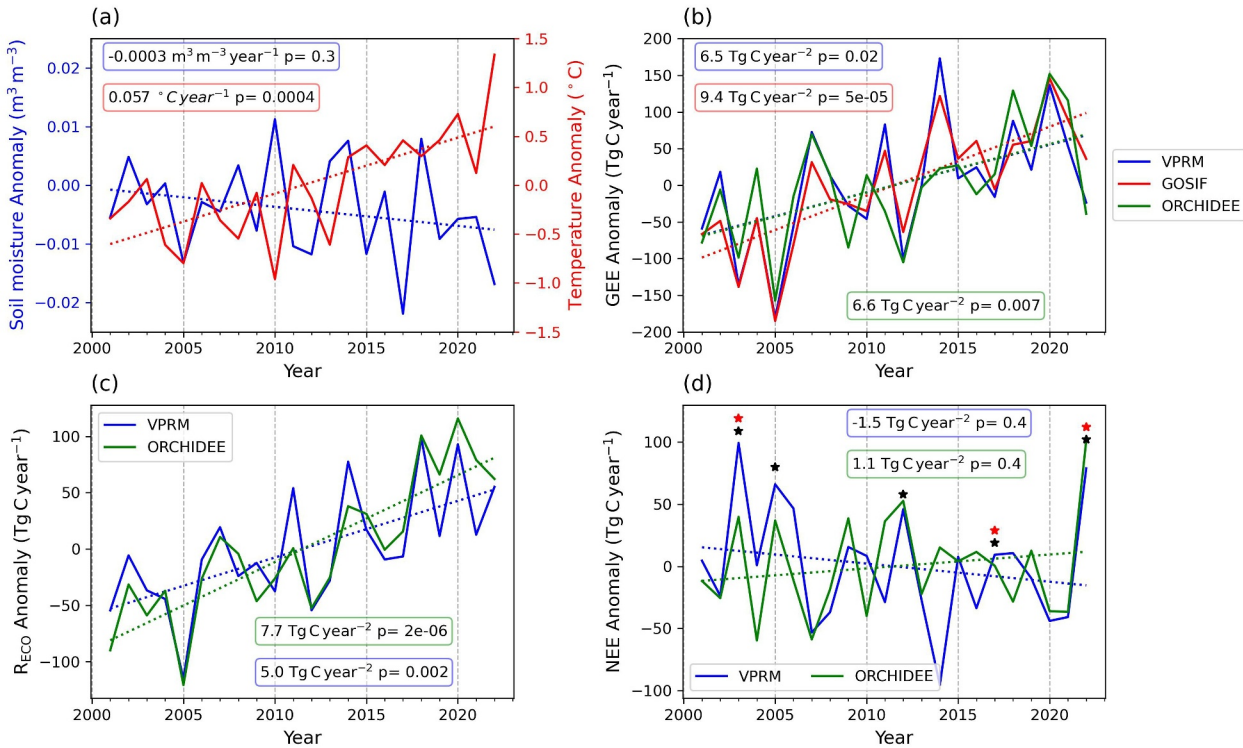

Figure 5. Time-series of annual anomalies over the study area. Annual anomalies in the climate data and carbon fluxes during 2001–2022. (a) Soil moisture and temperature, (b) GEE, (c) R_{ECO}, and (d) NEE aggregated over the entire study area. The dashed lines represent the trends, while in the boxes the trends and the p value are detailed. The black stars in subplot (d) mark the years in which the SPEI aggregated over 1-, 3-, 6-, 9-, or 12-month during summer is below −1, indicating a drought affecting most of the study area. The red stars mark the years when the summer temperature anomalies are above 1°C, indicating a summer heat event.

GOSIF and VPRM GEE show good agreement across biogeographical regions and climate drivers (Figure S7 in Supporting Information S1), confirming that VPRM is able to simulate the interannual variability of GEE well. ORCHIDEE and VPRM GEE present good agreement for most of the biogeographical regions and climate drivers (Figure S7 in Supporting Information S1), except for the Atlantic (ORHCIDEE presents higher positive correlations with T2M), the Alps (ORCHIDEE presents stronger negative correlations with SPEI01 to SPEI12, and SM2) and the Tyrrhenian-Adriatic (ORCHIDEE presents lower correlations with SPEI06 to SPEI12 and SM2). ORCHIDEE and VPRM R_{ECO} show good agreement across most biogeographical regions and climate drivers (Figure S8 in Supporting Information S1), except for the Italian sclerophyllous, Tyrrhenian-Adriatic, Apennine and Corsican montane regions where ORCHIDEE presents lower correlations with SPEI03 to SPEI12 (ORCHIDEE r = 0.17–0.56; VPRM r = 0.43–0.81) and SM2 (ORCHIDEE r = 0.22–0.45; VPRM r = 0.51–0.79).

Notably, the biogeographical regions where SPEI presents a stronger negative correlation with VPRM NEE anomalies are the Po Basin (r = −0.70 to −0.55) and the Italian sclerophyllous (r = −0.59 to −0.49) (Figure 7). For the other biogeographical regions, except the Alps, NEE anomalies present a weaker negative correlation with SPEI (between −0.54 and −0.17) and SM2 (between −0.32 and 0.07), compared with the positive correlations with GEE anomalies (SPEI: r = 0.37–0.76; SM2: r = 0.35–0.64).

3.4. Intra-Annual Variability of Carbon Fluxes

In the following section, we study the intra-annual variability of the carbon fluxes for two study cases. Figure 8a depicts the impact of the 2005 drought on carbon fluxes in the Iberian sclerophyllous region. VPRM indicates reduced GEE and R_{ECO} from late January to October. Higher GEE reductions of -2.0 ± 1.1 g C m^{-2} day^{-1} (the error corresponds to spatial standard deviation) appear in late April and May. GEE and R_{ECO} anomalies evolve similarly, although the impact on R_{ECO} is lower (-1.6 ± 0.8 g C m^{-2} day^{-1}). Climate driver anomalies (Figure 8c) reveal persistent negative soil moisture anomalies, dipping to -0.09 ± 0.02 m^{3}m^{-3} from the start of the year to

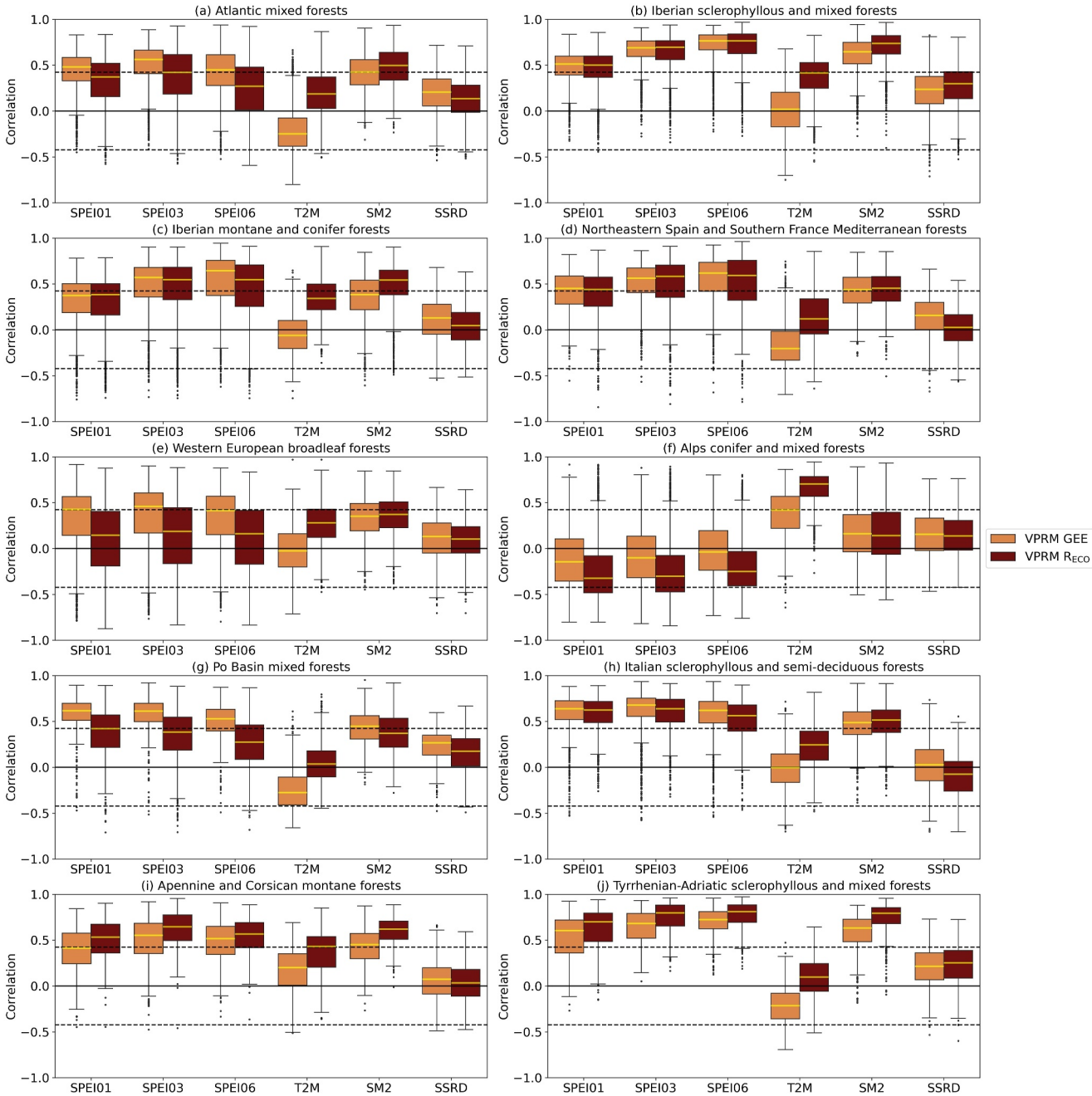

Figure 6. Drivers of carbon flux anomalies. Boxplots of correlation values between VPRM GEE and R_{ECO} detrended anomalies and the different climate drivers and drought indices aggregated over the growing season months for each biogeographical region. The median is represented by a yellow line. The discontinuous black lines represent the limit when correlations are significant ($p < 0.05$).

October, particularly during spring when fluxes are the lowest. Negative temperature anomalies (below −5°C) are observed during winter, delaying the start of the growing season, while May-July features positive temperature anomalies (>3°C), further depleting soil moisture. The event leads to a 65.5 Tg C year^{-1} (−25.4%) reduction in annual GEE, and 47.3 Tg C year^{-1} (−18.9%) decrease in annual R_{ECO}, resulting in a 18.1 Tg C year^{-1} (−251.0%) increase in NEE (i.e., decrease in net carbon uptake), and turning the ecosystems in the region from net carbon sinks into net carbon sources. The Atlantic, Iberian montane, north-eastern Spain and southern France regions also experience net carbon uptake reductions (Figure S9 in Supporting Information S1) of 14.0 Tg C year^{-1}

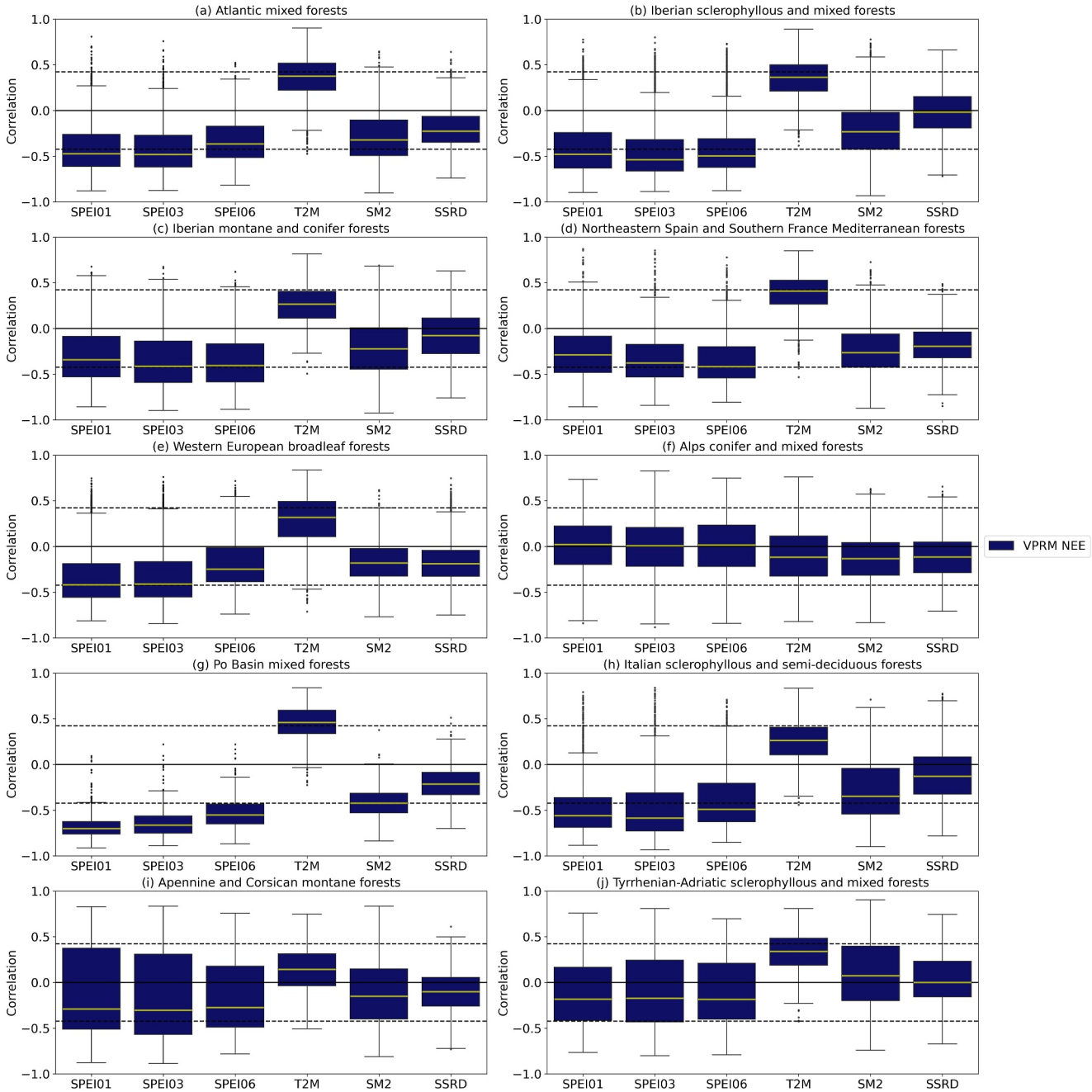

Figure 7. Drivers of NEE anomalies. As Figure 6 but for VPRM NEE.

(−16.1%), 6.8 Tg C year^{-1} (−35.6%) and 3.4 Tg C year^{-1} (−21.4%), respectively. In the south-western European region, the 2005 drought causes a total net carbon uptake reduction of 76.4 Tg C year^{-1} (−22.0%).

In 2022, south-western Europe experiences its hottest recorded summer, coupled with an extended drought event extending from winter until November (Copernicus Climate Change Service (C3S), 2023). Winter and spring precipitation and soil moisture deficits further increase during summer due to the unusually warmer temperatures and multiple heat wave episodes (Copernicus Climate Change Service (C3S), 2023). Figure 8b shows the 2022 spatial mean GEE and R_{ECO} anomalies in the Atlantic region. GEE remains persistently low from June to August, except for early July. R_{ECO} also shows negative summer anomalies, although for a shorter period and with smaller reductions than GEE. During spring, GEE and R_{ECO} experience positive anomalies (over 2.1 ± 0.9 g C m^{-2} day^{-1})

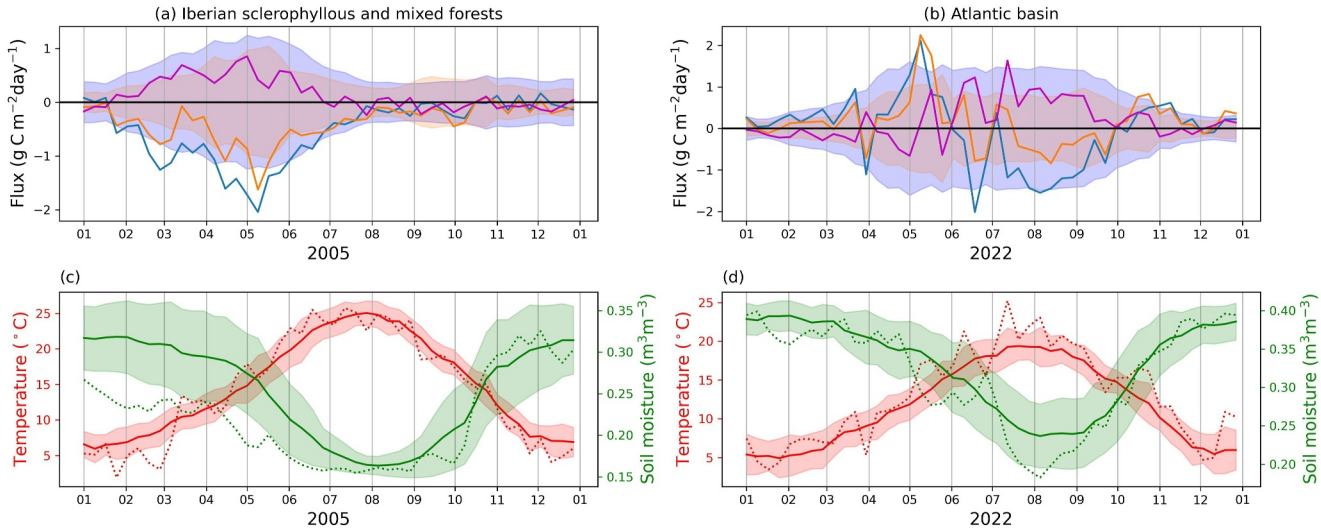

Figure 8. Intra-annual impact of heat and drought. Time series of the spatially average anomalies for the Iberian sclerophyllous in 2005 (a, c), and Atlantic mixed forest in 2022 (b, d) for (a, b) 8-day GEE (blue), R_{ECO} (orange), and NEE (pink). (c, d) Spatially averaged 8-day T2M (red) and SM2 (green) for the study year (dotted line) and the climatic mean for the 2001 to 2022 period (solid line). The shaded areas correspond to the temporal standard deviation for each 8-day period.

driven by the exceptionally high temperatures during May (over +4°C) (Figure 8d). The VPRM model estimates a decrease in the net carbon uptake of 16.2 Tg C year^{-1} (−18.7%) in the region during 2022 and 91.7 Tg C year^{-1} (−26.4%) in the south-western European domain.

4. Discussion

4.1. Long-Term Trends of Ecosystem Carbon Fluxes

In this study, we analyzed the long-term trends and interannual variability of carbon fluxes in the south-western European region from 2001 to 2022 to understand the response of these fluxes to heat and drought events. The statistical analysis of the carbon fluxes reveals an overall increase or stability of GEE (spatial median of 5.51, 3.58, and 3.58 g C m^{-2} year^{-2} for GOSIF, VPRM and ORCHIDEE, respectively) and R_{ECO} (3.01 and 4.02 g C m^{-2} year^{-2} for VPRM and ORCHIDEE, respectively). These trends are particularly prominent in montane regions such as the Alps, Apennines, Pyrenees, and Dinaric Alps. We identify a positive trend of the enhanced vegetation index (EVI) derived from MODIS surface reflectances (Vermote, 2015) over the Mediterranean region (trends up to 0.0012 EVI year^{-1}), which is more evident during the spring and winter months (Figure S10 in Supporting Information S1). Additionally, when examining long-term trends in the air temperatures using ERA5-Land data (Muñoz-Sabater, 2019) (Figure S11 in Supporting Information S1), a more substantial winter warming (up to 0.2°C year^{-1}) is observed over these same regions. The temperature rise during the colder season contributes to the increase in GEE and R_{ECO} values by alleviating growth limitations and extending the growing season (Keenan et al., 2016). This is supported by similar increases in GEE based on the GOSIF data set, which relies on satellite-derived SIF data (Li & Xiao, 2019), reinforcing the notion of elevated gross carbon uptake in high-altitude regions of the south-western European region.

However, differences between GOSIF, ORCHIDEE, and VPRM are observed in other biogeographical regions, possibly due to differences in model parameterization and input data. The discrepancies between the three models impair our ability to conclude about the long-term trends in NEE. GOSIF exhibits an overall higher spatial median compared to VPRM and ORCHIDEE. GOSIF solely relies on SIF data and an ensemble of SIF-GEE linear relationships computed from global flux tower data, whereas VPRM combines remotely sensed vegetation indices, meteorological data, and region-specific model parameters. Consequently, the long-term increase in GOSIF is directly linked to SIF data, whereas VPRM's response is influenced by both vegetation indices and climate drivers. On the contrary, ORCHIDEE depends solely on climate drivers, used to derive a dynamic vegetation model, which simulates processes that affect the carbon cycle, that is, photosynthesis, carbon allocation, maintenance and growth respiration, litter decomposition, and vegetation dynamics (McGrath

et al., 2023). ORCHIDEE simulations account for dynamic vegetation and time-varying carbon pools, as well as the input of atmospheric CO_2 concentrations and a dynamic nitrogen cycle which are not present in GOSIF and VPRM and are essential for long-term simulations of carbon fluxes (McGrath et al., 2023). However, because ORCHIDEE simulates phenology and vegetation dynamics, depending on calibrated parameters using global data, this adds uncertainty in the estimation of regional growing season onset and end, and limits the accuracy of long-term simulations of carbon fluxes (Santaren et al., 2014), which could explain the differences in the spatial distribution of the trends between VPRM and ORCHIDEE GEE.

According to VPRM simulations, R_{ECO} has also increased in the past two decades, at a slower rate than GEE but affecting a larger area (see Figure 3). The increase in R_{ECO}, especially in high-altitude regions, partially offsets the increase in GEE, resulting in only a modest increase in the carbon sink (0.69 g C m^{-2} $year^{-2}$). While ORCHIDEE estimates a modest decrease in the carbon sink (−0.51 g C m^{-2} $year^{-2}$) produced by a higher estimation of the R_{ECO} long-term trend, totally offsetting the increase in GEE. This balance suggests that the south-western Europe ecosystems maintain equilibrium between increased carbon uptake through photosynthesis and carbon released through respiration. Unlike temperate and boreal forests, which are experiencing a long-term increase in their carbon sink potential (Yang et al., 2023; Yu et al., 2022), the Mediterranean regions exhibit balanced long-term carbon cycle trends. Ongoing warming and drying trends in the regions may lead to uncompensated responses in GEE and R_{ECO}, causing variations in the NEE trends. For instance, we have identified with VPRM a positive trend in NEE (i.e., a decreasing trend in net carbon uptake) of croplands in the Central Massif of France (Figure 3e) coinciding spatially with a drying trend in the region (Figure S12 in Supporting Information S1) (X. Liu et al., 2021). These prospects could further compromise the net carbon sink capacity of other agricultural ecosystems in south-western Europe as the ongoing drying trend (Figure S12 in Supporting Information S1) affects other regions in the domain. These findings highlight the vulnerability of the south-western European region's carbon sink capacity to climate change, especially more frequent and intense droughts.

4.2. Heat and Drought Events Control the Interannual Variability of Carbon Fluxes

The analysis of the interannual variability in carbon fluxes emphasizes the significant influence of climatic drivers on the detrended anomalies of these fluxes. Across all the biogeographical regions, except for the Alps ecosystems, water availability emerges as the dominant climatic driver for interannual variability (see Figure 6). This is evident through the strong correlation observed between these fluxes and both soil moisture and the SPEI. The close agreement between VPRM, ORCHIDEE, and GOSIF correlations further supports the influence of soil moisture and SPEI on GEE variability. This alignment is notable, considering that initially, one might attribute this relationship to soil moisture as a driver of the VPRM model.

Analyzing the influence of climate drivers on GEE reveals a direct link between climate dryness and the extent to which droughts influence the interannual variability of GEE. The regions where the water balance plays a more important role in the interannual anomalies of the GEE during the growing season are the semi-arid regions of the Iberian and Tyrrhenian-Adriatic sclerophyllous and mixed forests (see Figure 6). In these regions, GEE is strongly correlated with the occurrence of droughts during the growing season and in the previous 6 months (from the previous autumn forward). These findings align with previous research by Gouveia et al. (2017), who noted that, during the month of May, Mediterranean dry vegetation communities, particularly croplands, present the highest correlations between the vegetation activity and the SPEI aggregated at time scales between 3 and 9 months. These regions have a high proportion of non-forest vegetation (more than 85% of the vegetated areas) and low annual precipitation (less than 800 mm), explaining the heightened sensitivity to soil moisture availability during periods of active vegetation growth (Vicente-Serrano, 2007). In contrast, the Alps, characterized by the low annual temperatures (3.8°C) and high precipitation levels (1,485 mm), exhibit a positive correlation with air temperature and negative correlations with SPEI and soil moisture. This pattern suggests that the Alps' vegetation faces continuous energy limitations and warmer temperatures and increased solar radiation tends to bring climatic conditions closer to the optimal temperatures for photosynthesis (between 18 and 22°C).

While increased air temperatures negatively impact GEE (except for the Alps), their impact on R_{ECO} is less pronounced. These differences can be attributed to distinct ecophysiological responses of photosynthesis and respiration to temperature and soil moisture stress. Air temperature impacts photosynthesis when it surpasses a certain optimum temperature by reducing the chemical reaction kinetics (von Buttlar et al., 2018), whereas soil moisture stress impacts photosynthesis by ecophysiological and structural changes (Bréda et al., 2006). On the other hand,

increasing soil temperatures, and hence air temperatures, stimulates heterotrophic respiration by increasing the kinetics of soil microbial decomposition, root respiration and the diffusion of enzymes (von Buttlar et al., 2018), while strong soil moisture deficits produced by droughts negatively affects soil microbial activity and reduces autotrophic respiration due to the reduction of recently assimilated carbon (Migliavacca et al., 2011; Reichstein et al., 2003). Therefore, while an increase of temperature during the growing season can be negative for photosynthesis, especially if it is accompanied by a drought, the impact on R_{ECO} is reduced by the compensating effects. It is worth noting that these responses vary depending on the ecosystem type and plant species.

Our analysis reveals a higher influence of droughts on GEE anomalies compared with R_{ECO} anomalies in temperate humid regions such as the Atlantic, Western Europe, and the Po Basin regions. In contrast, the impacts of droughts on GEE and R_{ECO} in other Mediterranean climate regions show similar or higher correlations with R_{ECO}. The different responses of GEE and R_{ECO} to drought occurrences between humid and dry climates may be attributed to various factors, including higher intra-annual compensation effect for R_{ECO} compared to GEE in humid regions, the resistance capacity of Mediterranean vegetation to seasonal droughts (Gazol et al., 2018), and lagged responses of R_{ECO} to drought compared to more immediate effects on GEE (Ryan & Law, 2005). These findings align with previous studies on the 2003 summer drought and heat event in Central Europe (Ciais et al., 2005; Reichstein et al., 2007), which reported a higher impact of drought on GEE compared to R_{ECO} in temperate ecosystems. We note that temperate humid regions in the Italian Peninsula exhibit the highest influence of droughts on the NEE variability during the growing season. Consequently, anomalies in NEE are highly influenced by droughts in these regions compared with Mediterranean regions (Figure 7). These results emphasize the vulnerability of the south-western Europe's net carbon sink to drought occurrences.

4.3. Warm Springs Do Not Compensate the Decreasing Effect of Droughts on CO_2 Fluxes

We find that both GEE and R_{ECO} decrease during the summer for Atlantic mixed forests in 2022. This can be explained by the heat wave in conjunction with persistent drought conditions (Bastos et al., 2014; García-Herrera et al., 2010) as shown by several studies on the coupled effects of heat and water stress on the photosynthetic capacity of southern European ecosystems (Bastos et al., 2014; Ciais et al., 2005; Ermitão et al., 2021; Reichstein et al., 2007).

However, the impact of heat-drought combined conditions on R_{ECO} is lower than on GEE. These differential responses between GEE and R_{ECO} result in a reduction of the net carbon uptake capacity of the ecosystems and turn ecosystems from net carbon sinks to carbon sources (Ciais et al., 2005). These results align with the ones obtained by a previous study (von Buttlar et al., 2018) that found that the combination of drought and heat typically led to a strong decrease in GEE, whereas heat and drought impacts on respiration partially offset each other using eddy-covariance flux measurements.

For the 2022 study case, we find that the impact of summer heat and drought events is partially compensated by abnormally warm temperatures between April and June, which leads to an increase in GEE and R_{ECO}. The warm spring temperatures produce similar positive anomalies in GEE and R_{ECO}. The high spring R_{ECO} anomaly detected in these two study cases could be attributed to the combination of high spring temperatures and the high GEE anomalies at the peak of the growing season, causing an increase in the respiration of the recently assimilated carbon. The similar increment of the GEE and R_{ECO} during spring compensates for each other, resulting in a minimal NEE anomaly during the spring.

These distinct seasonal compensation effects between spring and summer lead to an overall reduction in net carbon uptake compared to normal values during the growing season, dominating the anomalies for the entire year. These findings highlight the importance of studying the combined impacts of heat and drought events on both GEE and R_{ECO}, as they can cause non-linear effects on the terrestrial carbon balance. Focusing solely on GEE might underestimate the true impact of heat and drought events on ecosystems, and the terrestrial carbon balance.

These results suggest that the Mediterranean ecosystems, adapted to recurrent seasonal droughts during the summer (Peñuelas & Sardans, 2021), are more vulnerable to the occurrence of persistent soil moisture deficits at the beginning of the growing season, especially if persistent drought conditions affect the previous humid seasons. The Iberian sclerophyllous region is principally cultivated with winter crops (Gouveia et al., 2017), which can be affected by water deficits at early stages of crop development. Moreover, the cold winter conditions during 2005 in the Iberian Peninsula (anomalies of −5°C) may have also affected GEE by delaying the start of the

growing season or with a direct frost damage. These results highlight the potential recurrent stress that will suffer the Iberian ecosystems under future climate scenarios, and the compromised carbon balance from these ecosystems (Moemken et al., 2022).

4.4. VPRM Modifications Improve the Response of Carbon Fluxes to Heat and Drought

We modified the data-driven biosphere model VPRM for GEE and R_{ECO} parameterizations, incorporating plant functional type-specific parameters calibrated using data solely from flux tower stations in the southern Europe and neighboring regions. These modifications include the inclusion of soil moisture-related water stress in the GEE parameterization, resulting in improved model GEE estimates that better align with changes between energy and water-limited regimes. This modification improves the correlation between modeled and tower GEE estimates at the monthly timescale in evergreen-leaf ecosystems, such as evergreen forests (Figure S4b in Supporting Information S1). Additionally, we implemented a more sophisticated semi-empirical R_{ECO} parameterization that considers vegetation productivity (GEE) and soil moisture, enhancing the predictive capability of the model to better analyze seasonal and annual variations of the carbon balance.

However, several limitations emerge from the VPRM model for long-term biogenic flux studies. For instance, the VPRM model relies on a land cover map based on the Synergetic Land Cover Product (SYNMAP) (Jung et al., 2006), which joins three global land cover products based on satellite observations as recent as 2001, failing to account for land-use/land-cover changes during the 2001 to 2022 period. This limitation could be solved by incorporating dynamic land-cover maps as the MODIS MCD12Q1 product (Friedl & Sulla-Menashe, 2019). Moreover, the application of static parameters for each PFT for the 2001 to 2022 period could not properly capture the increase in the light-use-efficiency factor due to the atmospheric CO_2 fertilization effect or nitrogen deposition (Keenan et al., 2016). A dynamic set of VPRM parameters, updated every few years, could address this issue, provided that a continuous and standardized data set of carbon flux tower observations encompassing various biogeographical regions, climates and PFT becomes available. Despite the commendable efforts of organizations like FLUXNET (Pastorello et al., 2020) and the Integrated Carbon Observation System (ICOS), certain biomes and PFT remain underrepresented in observation data sets, as it is the case of mixed forests and shrublands, which only are represented by 1 and 2 flux towers, respectively. This underrepresentation contributes to model uncertainties in estimating carbon fluxes in these regions, evidenced by the low model performance for these PFTs (Figure 2). The VPRM predicting capabilities and the analysis of the carbon balance would benefit from the incorporation of additional flux tower sites in these underrepresented biomes and PFT.

Despite the enhancements made to the R_{ECO} parameterization, the model evaluation reveals moderate correlations with R_{ECO} observations compared to GEE and NEE (Figure S4 in Supporting Information S1). This discrepancy suggests the existence of unaccounted processes within the model. These processes could relate to carbon pool size (Reichstein et al., 2003), the maximum leaf area index throughout the year, nitrogen deposition, and stand age (Migliavacca et al., 2011) in natural ecosystems. In the case of croplands, factors such as management practices and soil carbon pools could potentially influence respiration (Eugster et al., 2010). Addressing these aspects could improve R_{ECO} estimation but may introduce additional sources of model uncertainty due to increased complexity.

5. Conclusions

Using a modified VPRM model with parameters optimized for south-western European ecosystems, this study analyzed the long-term trends and interannual variability of carbon fluxes in south-western Europe from 2001 to 2022 to understand the response of these fluxes to heat and drought events. Our results revealed high spatial variations of the carbon flux trends, being higher over mountainous regions in the Alps, Apennine, and Corsican montane forests. Similar increases in the ecosystem's photosynthesis and respiration compensate each other, resulting in only a modest increase of 0.69 g C m^{-2} $year^{-2}$ (spatial median) in net carbon uptake over the region. Ongoing warming and drying trends in the region may lead to uncorrelated responses in gross ecosystem exchange and ecosystem respiration, reverting the trend in the net ecosystem exchange. These findings highlight the vulnerability of the south-western Europe's carbon sink capacity to potential shifts in climate change, especially more frequent and intense droughts.

Analyzing the influence of climate drivers on the gross ecosystem exchange and respiration reveals a direct link between climate dryness and the extent to which droughts influence the interannual variability of the carbon fluxes. Water balance plays a more important role in the interannual anomalies of the gross ecosystem exchange and

respiration during the growing season in the semi-arid Iberian and Tyrrhenian-Adriatic sclerophyllous regions. However, this analysis reveals a higher drought influence on gross ecosystem exchange anomalies than on ecosystem respiration anomalies in temperate humid regions such as the Atlantic, Western Europe, and the Po Basin. These findings emphasize the importance of studying the combined impacts of heat and drought events on both ecosystem photosynthesis and respiration, as they can cause non-linear impacts on the terrestrial carbon balance.

Data Availability Statement

The VPRM version with the modifications detailed in this study is available in a Python program in the repository "Vegetation Photosynthesis and Respiration Model code and output for south-western Europe between 2001 and 2022" at Zenodo, via https://doi.org/10.5281/zenodo.10782550 with Creative Commons Attribution 4.0 International license (Villalba, 2024). In this repository, there are also the terrestrial ecosystem carbon fluxes estimated with the modified VPRM over the south-western Europe domain between 2001 and 2022 used in this study in NetCDF format. The hourly ERA5-Land data (Muñoz-Sabater, 2019) was downloaded from the Copernicus Climate Change Service (C3S) Climate Data Store (2022). Neither the European Commission nor ECMWF is responsible for any use that may be made of the Copernicus information or data it contains. The MODIS MOD09A1 v6.1 product used for deriving the remotely sensed vegetation indices in this study is available at the NASA EOSDIS Land Processes Distributed Active Archive Center via https://doi.org/10.5067/MODIS/MOD09A1.061.

Acknowledgments
This work has been made possible thanks to the financial support of the European Research Council (ERC) Consolidator project: Integrated System Analysis of Urban Vegetation and Agriculture (818002-URBAG), the Spanish Ministry of Science, Innovation and Universities, Through the "Maria de Maeztu" programme for Units of Excellence (CEX2019-000940-M), and the funding and recognition awarded to research group Sostenipra (2021 SGR 00734) by the Department of Research and Universities of the Generalitat de Catalunya. The authors thankfully acknowledge the computer resources at PICASSO and the technical support provided by the Universidad de Málaga (RES-AECT-2020-2-0004). This work used eddy-covariance data acquired and shared by the FLUXNET community, including these networks: AmeriFlux, AfriFlux, AsiaFlux, CarboAfrica, CarboEuropeIP, CarboItaly, CarboMont, ChinaFlux, Fluxnet-Canada, GreenGrass, ICOS, KoFlux, LBA, NECC, OzFlux-TERN, TCOS-Siberia, and USCCC. The FLUXNET eddy-covariance data processing and harmonization was carried out by the ICOS Ecosystem Thematic Center, AmeriFlux Management Project and Fluxdata project of FLUXNET. The authors thank Dr. Fabienne Maignan, Dr. Philippe Peylin and Vladislav Bastrikov, and their research group in the LSCE for the ORCHIDEE simulations output. The authors also thank the ICOS Infrastructure for support in collecting and curating the flux tower data. T. Lauvaux was supported by the French National Chair program Carbon Across Scales and Landscapes (CASAL).

References

Alonso, D., Gouveia, C. M., Russo, A., & Páscoa, P. (2019). Crop's exposure, sensitivity and adaptive capacity to drought occurrence. *Natural Hazards and Earth System Sciences*, *19*(2), 2727–2743. https://doi.org/10.5194/nhess-19-2727-2019

Bastos, A., Gouveia, C. M., Trigo, R. M., & Running, S. W. (2014). Analysing the spatio-temporal impacts of the 2003 and 2010 extreme heatwaves on plant productivity in Europe. *Biogeosciences*, *11*(13), 3421–3435. https://doi.org/10.5194/bg-11-3421-2014

Bento, V. A., Russo, A., Vieira, I., & Gouveia, C. M. (2023). Identification of forest vulnerability to droughts in the Iberian Peninsula. *Theoretical and Applied Climatology*, *152*(1), 559–579. https://doi.org/10.1007/s00704-023-04427-y

Bréda, N., Huc, R., Granier, A., & Dreyer, E. (2006). Temperate forest trees and stands under severe drought: A review of ecophysiological responses, adaptation processes and long-term consequences. *Annals of Forest Science*, *63*(6), 625–644. https://doi.org/10.1051/forest:2006042

Ciais, P., Reichstein, M., Viovy, N., Granier, A., Ogée, J., Allard, V., et al. (2005). Europe-wide reduction in primary productivity caused by the heat and drought in 2003. *Nature*, *437*(7058), 529–533. https://doi.org/10.1038/nature03972

Ciais, P., Tan, J., Wang, X., Roedenbeck, C., Chevallier, F., Piao, S.-L., et al. (2019). Five decades of northern land carbon uptake revealed by the interhemispheric CO_2 gradient. *Nature*, *568*(7751), 221–225. https://doi.org/10.1038/s41586-019-1078-6

Copernicus Climate Change Service (C3S). (2022). ERA5-Land hourly data from 1950 to present [Dataset]. *Copernicus Climate Change Service (C3S) Climate Data Store (CDS)*. https://doi.org/10.24381/CDS.68D2BB30

Copernicus Climate Change Service (C3S). (2023). European state of the climate 2022. *Copernicus Climate Change Service (C3S)*. https://doi.org/10.24381/GVAF-H066

Dayalu, A., Munger, J. W., Wofsy, S. C., Wang, Y., Nehrkorn, T., Zhao, Y., et al. (2018). Assessing biotic contributions to CO_2 fluxes in northern China using the Vegetation, Photosynthesis and Respiration Model (VPRM-CHINA) and observations from 2005 to 2009. *Biogeosciences*, *15*(21), 6713–6729. https://doi.org/10.5194/bg-15-6713-2018

Ermitão, T., Gouveia, C. M., Bastos, A., & Russo, A. C. (2021). Vegetation productivity losses linked to Mediterranean hot and dry events. *Remote Sensing*, *13*(19), 4010. https://doi.org/10.3390/rs13194010

Eugster, W., Moffat, A. M., Ceschia, E., Aubinet, M., Ammann, C., Osborne, B., et al. (2010). Management effects on European cropland respiration. *Agriculture, Ecosystems & Environment*, *139*(3), 346–362. https://doi.org/10.1016/j.agee.2010.09.001

Fernández-Martínez, M., Peñuelas, J., Chevallier, F., Ciais, P., Obersteiner, M., Rödenbeck, C., et al. (2023). Diagnosing destabilization risk in global land carbon sinks. *Nature*, *615*(7954), 848–853. https://doi.org/10.1038/s41586-023-05725-1

Fischer, E. M., & Schär, C. (2010). Consistent geographical patterns of changes in high-impact European heatwaves. *Nature Geoscience*, *3*(6), 398–403. https://doi.org/10.1038/ngeo866

Friedl, M., & Sulla-Menashe, D. (2019). MCD12Q1 MODIS/Terra+Aqua land cover type yearly L3 global 500m SIN grid V006 [Dataset]. *NASA EOSDIS Land Processes Distributed Active Archive Center*. https://doi.org/10.5067/MODIS/MCD12Q1.006

Fu, Z., Ciais, P., Makowski, D., Bastos, A., Stoy, P. C., Ibrom, A., et al. (2022). Uncovering the critical soil moisture thresholds of plant water stress for European ecosystems. *Global Change Biology*, *28*(6), 2111–2123. https://doi.org/10.1111/gcb.16050

García-Herrera, R., Díaz, J., Trigo, R. M., Luterbacher, J., & Fischer, E. M. (2010). A review of the European summer heat wave of 2003. *Critical Reviews in Environmental Science and Technology*, *40*(4), 267–306. https://doi.org/10.1080/10643380802238137

Gazol, A., Camarero, J. J., Vicente-Serrano, S. M., Sánchez-Salguero, R., Gutiérrez, E., de Luis, M., et al. (2018). Forest resilience to drought varies across biomes. *Global Change Biology*, *24*(5), 2143–2158. https://doi.org/10.1111/gcb.14082

Gilabert, M. A., Moreno, A., Maselli, F., Martínez, B., Chiesi, M., Sánchez-Ruiz, S., et al. (2015). Daily GPP estimates in Mediterranean ecosystems by combining remote sensing and meteorological data. *ISPRS Journal of Photogrammetry and Remote Sensing*, *102*, 184–197. https://doi.org/10.1016/j.isprsjprs.2015.01.017

Giorgi, F., & Lionello, P. (2008). Climate change projections for the Mediterranean region. *Global and Planetary Change*, *63*(2–3), 90–104. https://doi.org/10.1016/j.gloplacha.2007.09.005

Gourdji, S. M., Karion, A., Lopez-Coto, I., Ghosh, S., Mueller, K. L., Zhou, Y., et al. (2022). A modified vegetation photosynthesis and respiration model (VPRM) for the eastern USA and Canada, evaluated with comparison to atmospheric observations and other biospheric models. *Journal of Geophysical Research: Biogeosciences*, *127*(1), e2021JG006290. https://doi.org/10.1029/2021JG006290

Gouveia, C. M., Trigo, R. M., Beguería, S., & Vicente-Serrano, S. M. (2017). Drought impacts on vegetation activity in the Mediterranean region: An assessment using remote sensing data and multi-scale drought indicators. *Global and Planetary Change*, *151*, 15–27. https://doi.org/10.1016/j.gloplacha.2016.06.011

Jin, H., Vicente-Serrano, S. M., Tian, F., Cai, Z., Conradt, T., Boincean, B., et al. (2023). Higher vegetation sensitivity to meteorological drought in autumn than spring across European biomes. *Communications Earth & Environment*, *4*(1), 299. https://doi.org/10.1038/s43247-023-00960-w

Jung, M., Henkel, K., Herold, M., & Churkina, G. (2006). Exploiting synergies of global land cover products for carbon cycle modeling. *Remote Sensing of Environment*, *101*(4), 534–553. https://doi.org/10.1016/j.rse.2006.01.020

Keenan, T. F., Prentice, I. C., Canadell, J. G., Williams, C. A., Wang, H., Raupach, M., & Collatz, G. J. (2016). Recent pause in the growth rate of atmospheric CO_2 due to enhanced terrestrial carbon uptake. *Nature Communications*, *7*(1), 13428. https://doi.org/10.1038/ncomms13428

Kobayashi, K., & Salam, M. U. (2000). Comparing simulated and measured values using mean squared deviation and its components. *Agronomy Journal*, *92*(2), 345. https://doi.org/10.1007/s100870050043

Li, X., & Xiao, J. (2019). Mapping photosynthesis solely from solar-induced chlorophyll fluorescence: A global, fine-resolution dataset of gross primary production derived from OCO-2. *Remote Sensing*, *11*(21), 2563. https://doi.org/10.3390/rs11212563

Liu, W., Zhang, Z., & Wan, S. (2009). Predominant role of water in regulating soil and microbial respiration and their responses to climate change in a semiarid grassland. *Global Change Biology*, *15*(1), 184–195. https://doi.org/10.1111/j.1365-2486.2008.01728.x

Liu, X., He, B., Guo, L., Huang, L., Yuan, W., Chen, X., et al. (2021). European carbon uptake has not benefited from vegetation greening. *Geophysical Research Letters*, *48*(20), e2021GL094870. https://doi.org/10.1029/2021GL094870

Los, S. O. (2013). Analysis of trends in fused AVHRR and MODIS NDVI data for 1982–2006: Indication for a CO_2 fertilization effect in global vegetation. *Global Biogeochemical Cycles*, *27*(2), 318–330. https://doi.org/10.1002/gbc.20027

Lv, Y., Liu, J., He, W., Zhou, Y., Tu Nguyen, N., Bi, W., et al. (2023). How well do light-use efficiency models capture large-scale drought impacts on vegetation productivity compared with data-driven estimates? *Ecological Indicators*, *146*, 109739. https://doi.org/10.1016/j.ecolind.2022.109739

Mahadevan, P., Wofsy, S. C., Matross, D. M., Xiao, X., Dunn, A. L., Lin, J. C., et al. (2008). A satellite-based biosphere parameterization for net ecosystem CO_2 exchange: Vegetation Photosynthesis and Respiration Model (VPRM). *Global Biogeochemical Cycles*, *22*(2). https://doi.org/10.1029/2006GB002735

Maselli, F., Papale, D., Puletti, N., Chirici, G., & Corona, P. (2009). Combining remote sensing and ancillary data to monitor the gross productivity of water-limited forest ecosystems. *Remote Sensing of Environment*, *113*(3), 657–667. https://doi.org/10.1016/j.rse.2008.11.008

McGrath, M. J., Petrescu, A. M. R., Peylin, P., Andrew, R. M., Matthews, B., Dentener, F., et al. (2023). The consolidated European synthesis of CO_2 emissions and removals for the European Union and United Kingdom: 1990–2020. *Earth System Science Data*, *15*(10), 4295–4370. https://doi.org/10.5194/essd-15-4295-2023

Migliavacca, M., Reichstein, M., Richardson, A. D., Colombo, R., Sutton, M. A., Lasslop, G., et al. (2011). Semiempirical modeling of abiotic and biotic factors controlling ecosystem respiration across eddy covariance sites. *Global Change Biology*, *17*(1), 390–409. https://doi.org/10.1111/j.1365-2486.2010.02243.x

Moemken, J., Koerner, B., Ehmele, F., Feldmann, H., & Pinto, J. G. (2022). Recurrence of drought events over Iberia. Part II: Future changes using regional climate projections. *Tellus A: Dynamic Meteorology and Oceanography*, *74*(2022), 262. https://doi.org/10.16993/tellusa.52

Molina, M. O., Sánchez, E., & Gutiérrez, C. (2020). Future heat waves over the Mediterranean from an Euro-CORDEX regional climate model ensemble. *Scientific Reports*, *10*(1), 8801. https://doi.org/10.1038/s41598-020-65663-0

Muñoz-Sabater, J. (2019). ERA5-Land hourly data from 1950 to present [Dataset]. *Copernicus Climate Change Service (C3S) Climate Data Store (CDS)*. https://doi.org/10.24381/cds.e2161bac

Olson, D. M., Dinerstein, E., Wikramanayake, E. D., Burgess, N. D., Powell, G. V. N., Underwood, E. C., et al. (2001). Terrestrial ecoregions of the world: A new map of life on Earth: A new global map of terrestrial ecoregions provides an innovative tool for conserving biodiversity. *BioScience*, *51*(11), 933–938. https://doi.org/10.1641/0006-3568(2001)051[0933:TEOTWA]2.0.CO;2

Pastorello, G., Trotta, C., Canfora, E., Chu, H., Christianson, D., Cheah, Y.-W., et al. (2020). The FLUXNET2015 dataset and the ONEFlux processing pipeline for eddy covariance data. *Scientific Data*, *7*(1), 225. https://doi.org/10.1038/s41597-020-0534-3

Peñuelas, J., & Sardans, J. (2021). Global change and forest disturbances in the Mediterranean basin: Breakthroughs, knowledge gaps, and recommendations. *Forests*, *12*(5), 603. https://doi.org/10.3390/f12050603

Qiu, R., Li, X., Han, G., Xiao, J., Ma, X., & Gong, W. (2022). Monitoring drought impacts on crop productivity of the U.S. Midwest with solar-induced fluorescence: GOSIF outperforms GOME-2 SIF and MODIS NDVI, EVI, and NIRv. *Agricultural and Forest Meteorology*, *323*, 109038. https://doi.org/10.1016/j.agrformet.2022.109038

Qu, L.-P., Chen, J., Xiao, J., de Boeck, H. J., Dong, G., Jiang, S.-C., et al. (2024). The complexity of heatwaves impact on terrestrial ecosystem carbon fluxes: Factors, mechanisms and a multi-stage analytical approach. *Environmental Research*, *240*, 117495. https://doi.org/10.1016/j.envres.2023.117495

Reichstein, M., Bahn, M., Ciais, P., Frank, D., Mahecha, M. D., Seneviratne, S. I., et al. (2013). Climate extremes and the carbon cycle. *Nature*, *500*(7462), 287–295. https://doi.org/10.1038/nature12350

Reichstein, M., Ciais, P., Papale, D., Valentini, R., Running, S., Viovy, N., et al. (2007). Reduction of ecosystem productivity and respiration during the European summer 2003 climate anomaly: A joint flux tower, remote sensing and modelling analysis. *Global Change Biology*, *13*(3), 634–651. https://doi.org/10.1111/j.1365-2486.2006.01224.x

Reichstein, M., Rey, A., Freibauer, A., Tenhunen, J., Valentini, R., Banza, J., et al. (2003). Modeling temporal and large-scale spatial variability of soil respiration from soil water availability, temperature and vegetation productivity indices. *Global Biogeochemical Cycles*, *17*(4). https://doi.org/10.1029/2003GB002035

Ribeiro, A. F., Russo, A., Gouveia, C. M., Páscoa, P., & Pires, C. A. (2019). Probabilistic modeling of the dependence between rainfed crops and drought hazard. *Natural Hazards and Earth System Sciences*, *19*(12), 2795–2809. https://doi.org/10.5194/nhess-19-2795-2019

Rita, A., Camarero, J. J., Nolè, A., Borghetti, M., Brunetti, M., Pergola, N., et al. (2020). The impact of drought spells on forests depends on site conditions: The case of 2017 summer heat wave in southern Europe. *Global Change Biology*, *26*(2), 851–863. https://doi.org/10.1111/gcb.14825

Running, S. W., Nemani, R. R., Heinsch, F. A., Zhao, M., Reeves, M., & Hashimoto, H. (2004). A continuous satellite-derived measure of global terrestrial primary production. *BioScience*, *54*(6), 547–560. https://doi.org/10.1641/0006-3568(2004)054[0547:ACSMOG]2.0.CO;2

Ryan, M. G., & Law, B. E. (2005). Interpreting, measuring, and modeling soil respiration. *Biogeochemistry*, *73*(1), 3–27. https://doi.org/10.1007/s10533-004-5167-7

Santaren, D., Peylin, P., Bacour, C., Ciais, P., & Longdoz, B. (2014). Ecosystem model optimization using in situ flux observations: Benefit of Monte Carlo versus variational schemes and analyses of the year-to-year model performances. *Biogeosciences*, *11*(24), 7137–7158. https://doi.org/10.5194/bg-11-7137-2014

Schimel, D., Stephens, B. B., & Fisher, J. B. (2015). Effect of increasing CO_2 on the terrestrial carbon cycle. *Proceedings of the National Academy of Sciences of the United States of America*, *112*(2), 436–441. https://doi.org/10.1073/pnas.1407302112

Stocker, B. D., Zscheischler, J., Keenan, T. F., Prentice, I. C., Peñuelas, J., & Seneviratne, S. I. (2018). Quantifying soil moisture impacts on light use efficiency across biomes. *New Phytologist*, *218*(4), 1430–1449. https://doi.org/10.1111/nph.15123

Stocker, B. D., Zscheischler, J., Keenan, T. F., Prentice, I. C., Seneviratne, S. I., & Peñuelas, J. (2019). Drought impacts on terrestrial primary production underestimated by satellite monitoring. *Nature Geoscience*, *12*(4), 264–270. https://doi.org/10.1038/s41561-019-0318-6

Thornton, P. E., Lamarque, J.-F., Rosenbloom, N. A., & Mahowald, N. M. (2007). Influence of carbon-nitrogen cycle coupling on land model response to CO_2 fertilization and climate variability. *Global Biogeochemical Cycles*, *21*(4). https://doi.org/10.1029/2006GB002868

van der Woude, A. M., Peters, W., Joetzjer, E., Lafont, S., Koren, G., Ciais, P., et al. (2023). Temperature extremes of 2022 reduced carbon uptake by forests in Europe. *Nature Communications*, *14*(1), 6218. https://doi.org/10.1038/s41467-023-41851-0

Vermote, E. (2015). MOD09A1 MODIS/Terra surface reflectance 8-day L3 global 500m SIN grid V006 [Dataset]. *NASA EOSDIS Land Processes Distributed Active Archive Center*. https://doi.org/10.5067/MODIS/MOD09A1.006

Vicente-Serrano, S. M. (2007). Evaluating the impact of drought using remote sensing in a Mediterranean, semi-arid region. *Natural Hazards*, *40*(1), 173–208. https://doi.org/10.1007/s11069-006-0009-7

Vicente-Serrano, S. M., Beguería, S., & López-Moreno, J. I. (2010). A multiscalar drought index sensitive to global warming: The standardized precipitation evapotranspiration index. *Journal of Climate*, *23*(7), 1696–1718. https://doi.org/10.1175/2009JCLI2909.1

Vicente-Serrano, S. M., Gouveia, C. M., Camarero, J. J., Beguería, S., Trigo, R., López-Moreno, J. I., et al. (2013). Response of vegetation to drought time-scales across global land biomes. *Proceedings of the National Academy of Sciences of United States of America*, *110*(1), 52–57. https://doi.org/10.1073/pnas.1207068110

Villalba, G. (2024). Vegetation photosynthesis and respiration model code and output for south-western Europe between 2001 and 2022 [Dataset]. *Zenodo*. https://doi.org/10.5281/ZENODO.10782550

von Buttlar, J., Zscheischler, J., Rammig, A., Sippel, S., Reichstein, M., Knohl, A., et al. (2018). Impacts of droughts and extreme-temperature events on gross primary production and ecosystem respiration: A systematic assessment across ecosystems and climate zones. *Biogeosciences*, *15*(5), 1293–1318. https://doi.org/10.5194/bg-15-1293-2018

Vonk, M. A. (2024). SPEI: A simple Python package to calculate and visualize drought indices (v0.4.0). *Zenodo*. https://doi.org/10.5281/zenodo.10816741

Warm Winter 2020 Team & ICOS Ecosystem Thematic Centre. (2022). Warm winter 2020 ecosystem eddy covariance flux product for 73 stations in FLUXNET-Archive format—Release 2022-1 (1.0) [Dataset]. *ICOS Carbon Portal*. https://doi.org/10.18160/2G60-ZHAK

Xiao, J. F., Davis, K. J., Urban, N. M., & Keller, K. (2014). Uncertainty in model parameters and regional carbon fluxes: A model-data fusion approach. *Agricultural and Forest Meteorology*, *189–190*, 175–186. https://doi.org/10.1016/j.agrformet.2014.01.022

Xiao, J. F., Davis, K. J., Urban, N. M., Keller, K., & Saliendra, N. Z. (2011). Upscaling carbon fluxes from towers to the regional scale: Influence of parameter variability and land cover representation on regional flux estimates. *Journal of Geophysical Research*, *116*(G3), G03027. https://doi.org/10.1029/2010JG001568

Yang, H., Ciais, P., Frappart, F., Li, X., Brandt, M., Fensholt, R., et al. (2023). Global increase in biomass carbon stock dominated by growth of northern young forests over past decade. *Nature Geoscience*, *16*(10), 886–892. https://doi.org/10.1038/s41561-023-01274-4

Yu, P., Zhou, T., Luo, H., Liu, X., Shi, P., Zhang, Y., et al. (2022). Global pattern of ecosystem respiration tendencies and its implications on terrestrial carbon sink potential. *Earth's Future*, *10*(8). https://doi.org/10.1029/2022EF002703

Zhu, Z., Piao, S., Myneni, R. B., Huang, M., Zeng, Z., Canadell, J. G., et al. (2016). Greening of the Earth and its drivers. *Nature Climate Change*, *6*(8), 791–795. https://doi.org/10.1038/nclimate3004

Zscheischler, J., Mahecha, M. D., von Buttlar, J., Harmeling, S., Jung, M., Rammig, A., et al. (2014). A few extreme events dominate global interannual variability in gross primary production. *Environmental Research Letters*, *9*(3), 035001. https://doi.org/10.1088/1748-9326/9/3/035001

Zscheischler, J., Reichstein, M., von Buttlar, J., Mu, M., Randerson, J. T., & Mahecha, M. D. (2014). Carbon cycle extremes during the 21st century in CMIP5 models: Future evolution and attribution to climatic drivers. *Geophysical Research Letters*, *41*(24), 8853–8861. https://doi.org/10.1002/2014GL062409

References From the Supporting Information

Ballabio, C., Panagos, P., & Monatanarella, L. (2016). Mapping topsoil physical properties at European scale using the LUCAS database. *Geoderma*, *261*, 110–123. https://doi.org/10.1016/j.geoderma.2015.07.006

ICOS RI. (2022). Ecosystem final quality (L2) product in ETC-Archive format—Release 2022-1 (1.0) [Dataset]. *ICOS ERIC—Carbon Portal*. https://doi.org/10.18160/PAD9-HQHU

Kountouris, P., Gerbig, C., Rödenbeck, C., Karstens, U., Koch, T. F., & Heimann, M. (2018). Technical note: Atmospheric CO_2 inversions on the mesoscale using data-driven prior uncertainties: Methodology and system evaluation. *Atmospheric Chemistry and Physics*, *18*(4), 3027–3045. https://doi.org/10.5194/acp-18-3027-2018

Reichstein, M., Falge, E., Baldocchi, D., Papale, D., Aubinet, M., Berbigier, P., et al. (2005). On the separation of net ecosystem exchange into assimilation and ecosystem respiration: Review and improved algorithm. *Global Change Biology*, *11*(9), 1424–1439. https://doi.org/10.1111/j.1365-2486.2005.001002.x

Saxton, K. E., & Rawls, W. J. (2006). Soil water characteristic estimates by texture and organic matter for hydrologic solutions. *Soil Science Society of America Journal*, *70*(5), 1569–1578. https://doi.org/10.2136/sssaj2005.0117

Virtanen, P., Gommers, R., Oliphant, T. E., Haberland, M., Reddy, T., Cournapeau, D., et al. (2020). SciPy 1.0: Fundamental algorithms for scientific computing in Python. *Nature Methods*, *17*(3), 261–272. https://doi.org/10.1038/s41592-019-0686-2

Webber, H., Ewert, F., Olesen, J. E., Müller, C., Fronzek, S., Ruane, A. C., et al. (2018). Diverging importance of drought stress for maize and winter wheat in Europe. *Nature Communications*, *9*(1), 4249. https://doi.org/10.1038/s41467-018-06525-2